
ADAPTIVE MOMENTUM AND NONLINEAR DAMPING FOR NEURAL NETWORK TRAINING

PREPRINT

Aikaterini Karoni
 School of Mathematics
 University of Bristol
 ve24580@bristol.ac.uk

Rajit Rajpal
 School of Mathematics
 University of Edinburgh
 s2592586@ed.ac.uk

Benedict Leimkuhler
 School of Mathematics
 University of Edinburgh
 b.leimkuhler@ed.ac.uk

Gabriel Stoltz
 CERMICS, Ecole Des Ponts, Institut polytechnique de Paris, CNRS, Marne-la-Vallée, France
 MATHERIALS team-project, Inria Paris, France
 gabriel.stoltz@enpc.fr

ABSTRACT

We propose a continuous-time scheme for large-scale optimization that introduces individual, adaptive momentum coefficients regulated by the kinetic energy of each model parameter. This approach automatically adjusts to local landscape curvature to maintain stability without sacrificing convergence speed. We demonstrate that our adaptive friction can be related to cubic damping, a suppression mechanism from structural dynamics. Furthermore, we introduce two specific optimization schemes by augmenting the continuous dynamics of mSGD and Adam with a cubic damping term. Empirically, our methods demonstrate robustness and match or outperform Adam on training ViT, BERT, and GPT2 tasks where mSGD typically struggles. We further provide theoretical results establishing the exponential convergence of the proposed schemes.

Keywords Optimization, Neural Networks, Large Language Models, Dynamical Systems, Transformers

1 Introduction

Neural network loss landscapes are highly non-convex, multi-modal and difficult to navigate [3, 15]. Improvements in training dynamics directly impact convergence speed, generalization performance, and computational cost. Momentum-based stochastic gradient methods are widely used to address these challenges. By maintaining exponentially weighted averages of past gradients, momentum stochastic gradient descent (mSGD) can help the optimization dynamics advance along flat regions, overcome barriers and control oscillations induced by stochastic gradients and ill-conditioning of the optimization landscape [30]. Recent work also shows that momentum can reduce stochastic-gradient bias [27]. In practice, this allows for larger and more robust learning rate choices than standard SGD. However, the inertia introduced through the momentum mechanism can itself become a new source of oscillations and instability.

When tuned appropriately, the momentum mechanism can help suppress oscillations in directions of high curvature and speed-up convergence in low-curvature regions. The standard practice deep learning is to keep the momentum coefficient fixed during training, despite the presence of highly coordinate-dependent curvature. In this work, we argue that the momentum coefficient should not remain fixed during training. Instead, it should be dynamically adapted to reflect the evolving kinetic energy of each parameter. Importantly, this adaptation should operate on a per-parameter basis to account for heterogeneity in the loss landscape.

The persistent performance gap between mSGD and Adam in training transformer architectures suggests that a single global momentum coefficient is often insufficient to handle the coordinate-wise variability of modern loss landscapes. Recent research has sought to explain this discrepancy [35, 13, 31, 34]. While one proposed explanation is that Adam is more robust to heavy-tailed gradient noise [34], recent work [13] demonstrates that Adam’s advantage persists even in

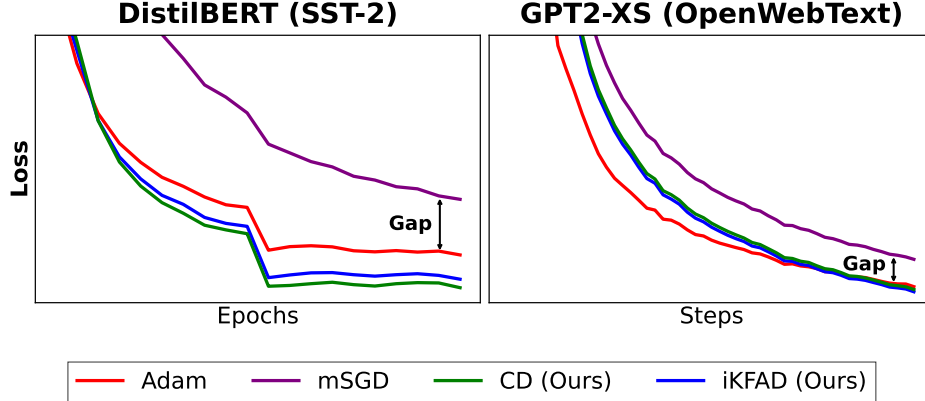


Figure 1: **Adam-mSGD gap:** Selected experiments demonstrating that CD and iKFAD can close the gap between Adam and mSGD without per-parameter adaptive learning rates on language modeling tasks using Transformers.

the full gradient setting, where it behaves similarly to sign descent with momentum. This suggests that Adam’s strength lies in its coordinate-wise normalization, which allows it to tackle the Hessian heterogeneity and anisotropic curvature that often cause mSGD to struggle [34]. As illustrated in Figure 1, our proposed damping mechanisms (CD and iKFAD) effectively bridge this gap in Transformer-based tasks without requiring explicit per-parameter adaptive learning rates.

To clarify the mechanics of our approach, we first establish the connection between momentum and friction (or damping). We begin with the discrete dynamics of mSGD [25], which can be written as

$$p_{n+1} = \mu p_n + \nabla f(x_n), \quad (1a)$$

$$x_{n+1} = x_n - \delta t p_{n+1}. \quad (1b)$$

In the zero–learning rate limit, these equations correspond to Linearly Dissipative Hamiltonian Dynamics (LDHD) [7, 16, 28]:

$$\dot{x} = p, \quad (2a)$$

$$\dot{p} = -\nabla f(x) - \gamma p, \quad (2b)$$

where $\gamma > 0$ is the friction coefficient. The “ $-\gamma p$ ” term introduces linear damping or friction into the dynamics. Conversely, applying an Euler discretization to the system (2) yields the discrete dynamics in (1) suggesting that the linear dissipation manifests as the exponentially weighted averaging of gradients characteristic of classical momentum. This relationship establishes a direct equivalence between the friction coefficient γ and the momentum coefficient μ through the relation

$$\mu = 1 - \gamma \sqrt{\delta t} \quad (3)$$

(see Appendix A). Consequently, the momentum coefficient μ in the discrete setting performs the exact same role as friction γ in continuous time: both regulate the momenta p and, by extension, the kinetic energy of the optimizer.

In continuous time the optimization process can therefore be viewed as the motion of a particle (whose coordinates correspond to the model parameters) navigating a potential field defined by the loss function $f(x)$. The state of the optimizer is defined by its position x and its momentum p , with the total system energy $H(x, p) = f(x) + \frac{1}{2} \|p\|^2$ representing the sum of the current loss (potential energy) and the squared norm of the momenta (kinetic energy). In a non-dissipative system ($\gamma = 0$), energy is conserved, causing the optimizer to oscillate perpetually around the minimum without settling. To achieve convergence, one must introduce dissipation to remove kinetic energy and allow the parameters to stabilize. While the momentum mechanism is often viewed as introducing exponentially weighted averages, this Hamiltonian perspective reframes it as a dissipative force. This $\mu - \gamma$ equivalence shows that a fixed momentum coefficient μ corresponds to applying the same damping across all coordinates. This fails to account for the heterogeneous structure of modern loss landscapes, where different parameters exhibit varying update velocities and require localized, adaptive damping to stabilize their individual trajectories.

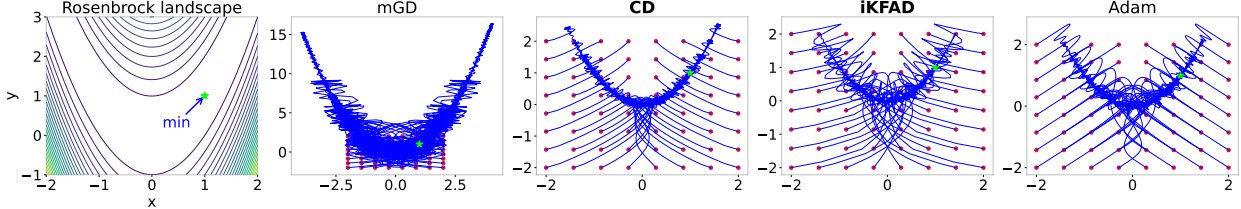


Figure 2: **Phase portraits for a two-dimensional Rosenbrock function:** Each red grid point corresponds to a different initialization in the (x, y) domain and each blue line corresponds to a different optimization trajectory. The minimum $(x_{\min}, y_{\min}) = (1, 1)$, is denoted by a green star. We set $\gamma = 1$, $h = 0.005$, and $\alpha = \rho = c = 1$. mSGD exhibits significant oscillations and overshooting of the minimum (note the different scale of the mSGD y-axis). In contrast, our per-parameter, adaptive friction method iKFAD and cubic damping method CD lead to smoother and much more direct trajectories towards the minimum, similarly to Adam.

Here, it is also useful to present the continuous dynamics of Adam [4], [8].¹

$$\dot{x} = \frac{p}{\sqrt{\zeta + \epsilon}}, \quad (4a)$$

$$\dot{p} = -\nabla f(x) - \gamma p, \quad (4b)$$

$$\dot{\zeta} = [\nabla f(x)]^2 - \alpha \zeta. \quad (4c)$$

Adam [11] employs the same momentum mechanism as mSGD that can potentially smooth out gradient oscillations and help the dynamics advance along flat regions and overcome barriers. In addition, Adam maintains an exponential moving average of squared gradients. While this quantity does not estimate curvature, it provides a crude diagonal approximation to the gradient second moment, enabling adaptive per-parameter learning rates that dampen updates in directions with high gradient variability.

Even though momentum-based methods commonly employ a fixed momentum coefficient, the choice of μ can significantly influence training dynamics and convergence speed. When tuned appropriately the momentum mechanism can help control oscillations, speed-up convergence in low-curvature regions, as well as overcome barriers. If not carefully chosen, the momentum mechanism can become the source of new oscillations, especially in directions of high curvature or introduce excessive damping to the system. Apart from using a time-independent (fixed) momentum coefficient, momentum-based methods also typically apply the same momentum coefficient across all parameters. This uniform treatment disregards directional differences in the local geometry of the loss landscape.

In this work, we argue for a dynamic and coordinate-wise adaptation of the momentum coefficient, that accounts for anisotropy in the optimization dynamics. Our iKFAD and CD methods can be thought of as replacing the constant friction coefficient in (2) with a coordinate-wise friction term. The resulting dynamics are of the following general form

$$\dot{x} = p, \quad (5a)$$

$$\dot{p} = -\nabla f(x) - g(p) \star p, \quad (5b)$$

where " \star ", denotes element-wise vector multiplication and $g : \mathbb{R} \rightarrow \mathbb{R}_{>0}$ is applied componentwise, i.e. $[g(p)]_i = g(p_i)$.

In order to qualitatively highlight the behavior of our optimizers, we examine their performance on two low-dimensional examples (see Figures 2 and 3 and observe that our methods are more stable than mGD and exhibit faster convergence in these simple settings.

2 Outline

The rest of this work is structured as follows. Section 3 introduces the continuous dynamics of three new optimizers (iKFAD, CD and Cadam) based on the aforementioned adaptive friction and cubic damping mechanism ideas. In Section 5, we examine the dynamical properties of the optimizers and show convergence of the continuous and discrete dynamics for iKFAD and CD. Finally, in Section 6 we present an empirical study of our methods on deep learning benchmarks.

¹We note that unlike LDHD-mSGD, this continuous-time version of Adam in Eq (4) doesn't have a direct correspondence to Adam [11], and does not include bias correction. However, it serves as a useful dynamical systems model of Adam as a damped system with per-parameter adaptive learning rates.

3 Methodology

The linear dissipation term $-\gamma p$ in Equation (2b) acts as a damping force on the momenta, with the value of the friction coefficient γ directly affecting their magnitude. Insufficient damping (low values of the friction parameter γ) can lead to high momenta, which can in turn result in oscillations and instability [22]. Excessive damping on the other hand (high values of γ), leads to excessive energy dissipation, small momenta and slow convergence. Having a friction or momentum coefficient that dynamically adapts based on the kinetic energy of the system would allow us to increase the damping when momenta are getting too high and decrease it when momenta are lower. This acts like a gentle thermostat on the system, allowing us to control the magnitude of the momenta. This adaptive friction mechanism was first introduced in the context of optimization in [9] with only a single adaptive coefficient for all parameters. Here, we modify the original dynamics, by introducing individual adaptive friction coefficients for each of the model parameters.

We refer to this new optimizer as *Individual Kinetic Friction Adaptive Descent (iKFAD)* and describe its dynamics as

$$\dot{x} = p, \quad (6a)$$

$$\dot{p} = -\nabla f(x) - \gamma p - \xi \star p, \quad (6b)$$

$$\dot{\xi} = \frac{[p]^2}{\rho} - \alpha \xi, \quad (6c)$$

where $\gamma, \alpha, \rho > 0$, $x, p, \xi \in \mathbb{R}^N$ and “ \star ”, “[.]^k” denote element-wise multiplication and exponentiation respectively. Note that while Equation (6b) also includes a standard fixed friction term apart from the new adaptive friction mechanism, we find that in practice we can often set $\gamma \approx 0$ and still maintain performance. The existence of a fixed friction term however is helpful in obtaining theoretical convergence guarantees. Note that iKFAD does not rescale individual learning rates like ADAM.

To better understand the role of the adaptive friction coefficient ξ , we look at the exact solution of equation (6c), given as

$$\xi(t) = e^{-\alpha t} \xi(0) + \frac{1}{\rho} \int_0^t [p(s)]^2 e^{-\alpha(t-s)} ds.$$

We see that ξ is an exponentially weighted average of the squares of past momenta, i.e. kinetic energies. Thus, a history of high momenta leads to an increased damping coefficient ξ , which helps “cool down” the system and control oscillatory behavior which might otherwise arise in the presence of high momenta. Conversely, a history of low momenta leads to less damping, allowing the optimizer to advance along low gradient, low-momenta regions.

In the discrete setting, we tend to think of Adam as performing per-parameter learning rate adaptation through the second-moment estimate ζ . In its continuous form (Equation (4)), Adam can be thought of as a method performing per-parameter momentum adaptation. We can therefore draw a parallel between iKFAD (6) and Adam. Both methods scale each element of the momentum vector individually, but while Adam does this in the x equation by dividing by the auxiliary variable ζ , iKFAD performs this adaptation in the momentum equation by applying adaptive, per-parameter damping on the momenta p through the adaptive friction ξ .

Our individual adaptive friction scheme addresses coordinate-wise anisotropy in the optimization dynamics in a manner analogous to the per-parameter learning rates used in adaptive optimizers such as Adam. While iKFAD does not explicitly rescale the gradient, the use of a separate friction coefficient for each parameter in the momentum update (6b) effectively regulates the update velocity on a per-coordinate basis. This is particularly relevant for architectures like Transformers, where parameters in different layers or attention heads exhibit vastly different update scales and noise characteristics, often limiting the effectiveness of mSGD’s global momentum. By introducing parameter-specific damping, iKFAD adaptively modulates the inertia of each parameter, allowing the optimizer to suppress oscillations in high-variance directions while maintaining progress in flatter regions, achieving a similar stabilizing effect to Adam.

Next, we consider the near-equilibrium behaviour of (6c). When α is sufficiently large and upon setting $\dot{\xi} \approx 0$, we obtain

$$\xi \approx (\alpha \rho)^{-1} [p]^2.$$

Substituting this approximation into (6b) yields

$$\dot{p} \approx -\nabla f(x) - (\alpha \rho)^{-1} [p]^3,$$

indicating that iKFAD behaves like a *cubically damped* momentum method in this regime. This motivates the study of the effect of cubic damping in state of the art optimizers such as mSGD and Adam. Cubic damping has long been studied as an effective vibration-suppression technique in engineering applications [23] [24][36][1]. Higher odd-order damping (such as quintic damping) would also be possible, provided that we use an odd power, so that the sign of the momenta is maintained.

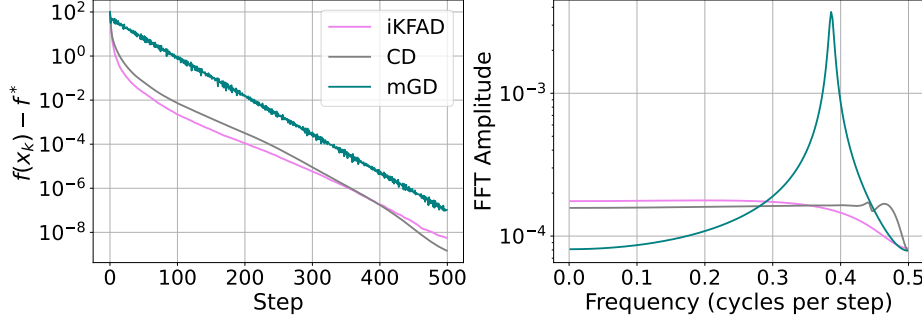


Figure 3: **Effect of adaptive friction and cubic damping on a two-hundred dimensional anisotropic quadratic:** $f(\mathbf{x}) = \frac{1}{2} \mathbf{x}^T \mathbf{A} \mathbf{x}$, with eigenvalues ranging between 1 and 10^4 . For momentum gradient descent (mGD), we choose the theoretically optimal learning rate $h = 2/\sqrt{M}$ and friction $\gamma = 2\sqrt{m}$, where $m = 1$ and $M = 10^4$ are the minimum and maximum eigenvalues of f respectively. **Left:** Objective function value $f(x)$ across optimization steps. Note that both iKFAD and CD outperform mGD in this setting. **Right:** Fourier spectrum of trajectory in direction of highest eigenvalue.

We first introduce *Cubically Damped mSGD* (CD), the dynamics of which are obtained by augmenting the momentum equation (2b) in LDHD by a cubic damping term.

$$\dot{x} = p, \quad (7a)$$

$$\dot{p} = -\nabla f(x) - \gamma p - c[p]^3. \quad (7b)$$

An advantage of the cubic damping mechanism is that it is more gentle than its linear counterpart for low momenta and becomes more aggressive than linear damping as momentum increases. This allows for gentler damping and therefore enhanced exploration along directions where gradients and momenta are low, while allowing for increased damping and oscillation control along high-momentum directions.

Figure 3 shows CD and iKFAD converging faster than theoretically optimal mGD on a 200-dimensional anisotropic quadratic function. Interestingly, mGD exhibits a pronounced spectral peak in the direction of the highest eigenvalue, while iKFAD and CD are able to significantly suppress oscillatory modes. Figure 2 shows phase portraits of various optimizers on the Rosenbrock function. For each optimizer, we initialize a grid of starting points (red dots) and plot the corresponding deterministic trajectories (blue lines). CD and iKFAD display strong suppression of oscillations akin to Adam, whereas mGD exhibits significant oscillations and overshooting of the minimum.

We now introduce our third optimizer, *Cubically damped Adam* (CADAM), the dynamics of which are obtained by augmenting the momentum equation in (4) by a cubic damping term:

$$\dot{x} = \frac{p}{\sqrt{\zeta + \epsilon}}, \quad (8a)$$

$$\dot{p} = -\nabla f(x) - \gamma p - c[p]^3, \quad (8b)$$

$$\dot{\zeta} = [\nabla f(x)]^2 - \alpha\zeta. \quad (8c)$$

To numerically integrate the continuous-time dynamics, we employ an *operator splitting* scheme. The key idea of operator splitting is to decompose the full vector field of the ODE into a sum of simpler sub-operators, each of which can be integrated exactly. The full update over one time step is then obtained by composing these partial flows, a type of splitting method (see [14]), although in practice an Euler-type discretization can be used of suitable modification of the dissipation coefficient is used. The explicit update rules for each step are provided in Appendix B.

In terms of memory and compute, CD maintains an identical memory footprint of $2N$ optimizer states (position and momentum) as mSGD, while adding only negligible computational overhead for the element-wise cubing of the momentum vector. Similarly, iKFAD and CADAM have the same memory requirements as Adam ($3N$) as they each maintain one additional auxiliary vector state variable (adaptive friction (ξ) for iKFAD and second-moment estimate (ζ) for CADAM).

4 Related Work

Although adaptation of the momentum hyperparameter μ has been suggested in prior works, the area remains relatively unexplored. The authors of [30] advocated for a gradual increase in the momentum coefficient as training progresses, based on the theoretical convergence results of [20, 21]. We provide a comparison of iKFAD against two known momentum schedules on FashionMNIST training with a ResNet18 in Appendix C. The authors of [29] derive a second-order ODE for Nesterov's accelerated gradient method, which also involves a time-dependent friction coefficient. In [9], an adaptive momentum coefficient based on the kinetic energy of the system was demonstrated (on molecular optimization) to lead to faster convergence and increased robustness with respect to the choice of learning rate compared to the use of a fixed momentum parameter. Adaptive friction has been studied in Langevin sampling, known as the Adaptive Langevin method [5, 26], which employs a thermostat to regulate noisy gradients. Controlling the momenta p to stabilize the optimization process and avoid oscillations has also been explored in [22], where the authors propose a momentum restart mechanism that resets the momenta to zero when oscillatory behavior emerges, typically once the momenta exceed a critical threshold. Rather than resetting momenta, iKFAD employs a continuous control mechanism that adapts the friction to keep the momenta within a stable range. In terms of theoretical work, [6] prove that choosing the friction parameter based on the smallest eigenvalue of the Hessian leads to convergence speed-ups in the case of strongly convex potentials.

5 Theoretical Results

This section establishes the convergence properties of iKFAD and CD. For strongly convex objective functions $f \in C^2$ with an bounds on the highest and lowest eigenvalues of the Hessian, we prove that the continuous-time dynamics of iKFAD and CD exhibit exponential convergence to the global minimum. We also demonstrate that this exponential convergence rate is preserved in the discrete-time schemes for a sufficiently small δt . We leave the convergence analysis of CADAM for future work.

5.1 iKFAD convergence analysis

Theorem 1. Consider a function $f \in C^2$ and assume that there exist $a, b > 0$ such that

$$\begin{aligned} a[f(x) - f(x^*)] + b\|x - x^*\|^2 \\ \leq (x - x^*) \cdot (\nabla f(x) - \nabla f(x^*)). \end{aligned} \tag{9}$$

Then, for any initial condition $(x_0, p_0, \xi_0) \in \mathbb{R}^d \times \mathbb{R}^d \times \mathbb{R}_+$, and considering $\gamma > 0$, there exist $\kappa > 0$ and $C \in \mathbb{R}_+$ such that the solution of (6) satisfies

$$f(x(t)) - f(x^*) + \|p(t)\| + \|\xi(t)\| \leq Ce^{-\kappa t}.$$

The condition (9) is satisfied for $f \in C^2$ with $0 < m \leq \nabla^2 f(x) \leq M < +\infty$. A similar condition is considered in [18].

Proof. See Appendix H.2 for the proof, which follows the same reasoning as the FAD continuous convergence proof in [9]. \square

Consider the splitting (17) of the continuous iKFAD dynamics and the integration scheme CDBA (see Table 2). The resulting discrete iKFAD dynamics can be written as

$$p_{n+1} = \beta_{n,\delta t} p_n - \delta t \nabla f(x_n), \tag{10a}$$

$$x_{n+1} = x_n + \delta t \beta_{n,\delta t} p_n - \delta t^2 \nabla f(x_n), \tag{10b}$$

$$\xi_{n+1} = e^{-\alpha \delta t} \left([\xi_n]^2 + \frac{(I - e^{-2\Xi_n \delta t}) [p_n]^2}{\rho} \right)^{1/2}, \tag{10c}$$

where $\Xi = \text{diag}(\xi)$ and $\beta_{n,\delta t} = e^{-(\gamma I + \Xi_n) \delta t}$ (see Appendix H.3 for more details). We can then state the following convergence result.

Theorem 2. Consider a function $f \in C^2$ satisfying $0 < m \leq \nabla^2 f(x) \leq M < +\infty$. Assume that $\gamma > 0$ and consider $L > 0$. Then, for any initial condition $(x_0, p_0, \xi_0) \in \mathbb{R}^d \times \mathbb{R}^d \times \mathbb{R}^d$ such that

$$\|x_0\| + \|p_0\| + \|\xi_0\| \leq L,$$

there exist $\delta t^* > 0$, $\kappa > 0$ and $C > 0$ (depending on L) such that $\forall \delta t \in (0, \delta t^*)$, $\forall n \geq 0$,

$$f(x_n) - f(x^*) + \|p_n\|^2 + \|\xi_n\|^2 \leq Ce^{-\kappa n \delta t}.$$

Proof. See Appendix H.3. The proof follows the strategy of the FAD discrete convergence analysis in [9].

5.2 CD convergence analysis

Theorem 3. Consider a function $f \in C^2$. Assume that $\gamma, c > 0$ and that there exist $a, b > 0$ such that

$$\begin{aligned} a[f(x) - f(x^*)] + b\|x - x^*\|^2 \\ \leq (x - x^*) \cdot (\nabla f(x) - \nabla f(x^*)). \end{aligned} \quad (11)$$

Then, for any initial condition $(x_0, p_0, \xi_0) \in \mathbb{R}^d \times \mathbb{R}^d \times \mathbb{R}_+$, there exist $\kappa > 0$ and $C \in \mathbb{R}_+$ such that the solution of (7) satisfies

$$f(x(t)) - f(x^*) + \|p(t)\| \leq Ce^{-\kappa t}.$$

Proof. See Appendix I.2.

Next, we consider an Euler discretization of (7), which is simpler to work with than the splitting scheme proposed in Table 2:

$$p_{n+1} = (1 - \gamma\delta t)p_n - c\delta t[p_n]^3 - \delta t\nabla f(x_n), \quad (12a)$$

$$x_{n+1} = x_n + \delta t p_n, \quad (12b)$$

where we assume that $\gamma\delta t$ is sufficiently small.

Theorem 4. Consider $f \in C^2$ and assume that there exist $m, M \in \mathbb{R}_+$ such that $m \leq \nabla^2 f(x) \leq M \forall x \in \mathbb{R}^N$. Fix $L > 0$, then, for any initial condition (x_0, p_0) such that $\|x_0\| + \|p_0\| \leq L$, there exists $\delta t^* > 0, r > 0$ and $C > 0$ for which

$$\begin{aligned} \forall n \geq 0 \text{ and } \forall \delta t \in (0, \delta t^*), \\ f(x_n) - f(x^*) + \|p_n\|^2 \leq Ce^{-\kappa n \delta t}. \end{aligned}$$

Proof. See Appendix I.3.

6 Numerical experiments

6.1 Results

To evaluate the performance of our proposed optimizers, we conduct a series of experiments across different machine learning tasks, including image classification on CIFAR-10 [12] using ResNet-18 and TinyViT [33], language classification with DistilBERT (66M) for SST-2 GLUE [32] and QNLI finetuning, and language generation via GPT2-Nano (0.85M) [10] as well as a custom GPT2-XS (45M). We downsized GPT2-S for computational efficiency by reducing the depth to 6 layers, number of heads to 8, and embedding dimension to 512. We refer to this as GPT2-XS. For language modeling experiments, we utilize a batch size of 16, following evidence that small batches can achieve performance comparable to larger scales [17], while TinyViT and ResNet-18 utilize a batch size of 128. We include comparisons against Adam and mSGD (standard implementations). We allocate equal resources to all optimizers during hyperparameter search. For a clean and simpler comparison, we omit common regularization and acceleration techniques such as learning rate scheduling, weight decay, and gradient accumulation. ResNet-18 results are reported in Appendix D, as all optimizers exhibited very similar performance in that setting. CADAM results are also discussed in Appendix E, as we did not observe a significant improvement in performance over Adam. A possible explanation is that cubic damping adds little if per-parameter learning rates are already being used.

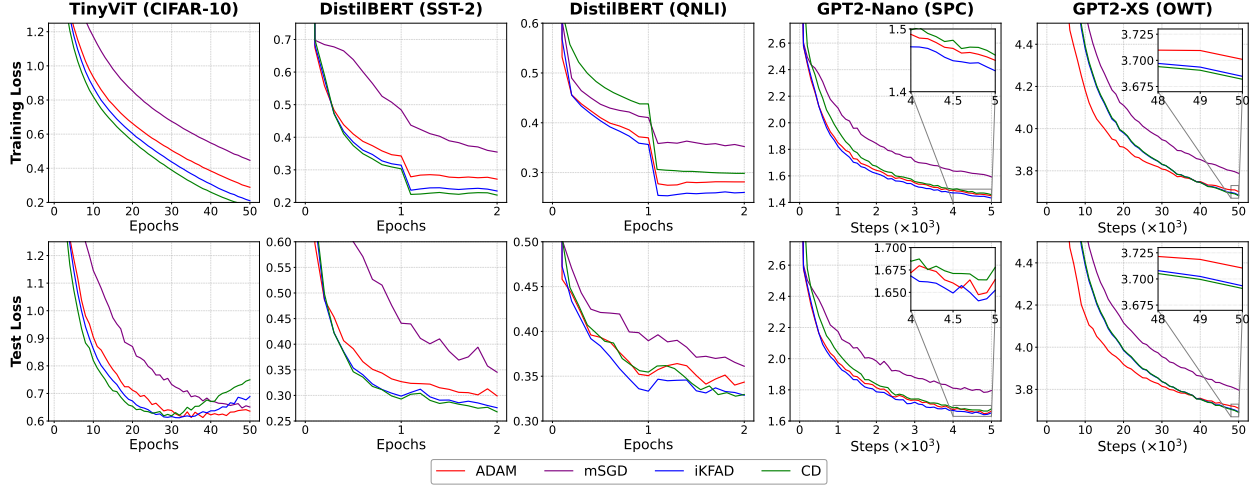


Figure 4: **Training and test losses** for iKFAD, CD, CADAM, Adam, and mSGD across ResNet-18, DistilBERT, and GPT2. All curves are averaged over 10 random seeds. Standard deviations are omitted for readability. All experiments showcase a substantial gap in performance between Adam and mSGD. Both iKFAD and CD are able to overcome this gap despite not using per-parameter learning rates.

Hyperparameter optimization for all schemes was conducted using Optuna Bayesian search with a fixed budget of 80 trials per experiment, with specific search ranges detailed in Appendix F. Our evaluation includes two distinct sweeps for the proposed optimizers—one with $\gamma > 0$ and one with $\gamma = 0$, selecting the top-performing configuration for each. Notably, CD and iKFAD exhibit similar performance (see Section 6.2). All the descriptions below pertain to Figure 4.

TinyViT. iKFAD and CD outperform Adam. They both reduce training loss faster and reach a slightly lower test loss. mSGD converges much more slowly, although it eventually approaches a similar test loss. We also note that the TinyViT accuracies obtained are competitive with those reported in [33] (without the use of distillation).

DistilBERT. There is a substantial performance gap between Adam and mSGD across both the SST-2 and QNLI tasks. On the SST-2 pretraining task, iKFAD and CD outperform Adam in both training and test loss. For the QNLI finetuning task, while a large gap persists between Adam and mSGD in training loss, the discrepancy in test loss is notably smaller. iKFAD reaches a lower test loss more rapidly, whereas CD initially follows Adam before eventually matching iKFAD’s test loss. We observe a sharp decline in training loss at the start of the second epoch, most noticeably in QNLI, which is not mirrored in the validation loss and suggests the onset of overfitting.

GPT2. We evaluated GPT2-Nano on Shakespeare and GPT2-XS on OpenWebText, and observe the same pattern across both benchmarks. The pronounced Adam-mSGD gap is visible in both scenarios. In GPT2-Nano, iKFAD exhibits accelerated convergence relative to Adam, while CD converges more gradually, ultimately matching the other optimizers toward the end of training. For GPT2-XS, the training and test loss trajectories of iKFAD and CD are nearly identical. This similarity may indicate that iKFAD operates near the steady state ($\xi \approx 0$), with the adaptive friction dynamics effectively behaving as a cubic damping.

Table 1: Best Test Loss results ($\mu \pm \sigma$).

Model (Dataset)	Adam	mSGD	CD	iKFAD
TinyViT (CIFAR-10)	0.613 ± 0.018	0.647 ± 0.012	0.619 ± 0.016	0.612 ± 0.014
DistilBERT (SST-2)	0.299 ± 0.012	0.345 ± 0.022	0.268 ± 0.009	0.276 ± 0.011
DistilBERT (QNLI)	0.340 ± 0.012	0.361 ± 0.016	0.328 ± 0.010	0.329 ± 0.013
GPT2-Nano (SPC)	1.647 ± 0.010	1.784 ± 0.011	1.664 ± 0.008	1.641 ± 0.006
GPT2-XS (OWT)	3.710 ± 0.011	3.797 ± 0.008	3.691 ± 0.016	3.693 ± 0.018

Across all benchmarks, iKFAD, CD, and CADAM consistently achieve lower training and test losses than Adam and mSGD, as well as higher accuracies. While we observe a persistent performance gap between fully-tuned mSGD and Adam in all language modeling tasks, our nonlinear damping mechanisms effectively bridge this discrepancy. Table 1 summarizes the best losses averaged over ten runs in each experiment along with the corresponding standard deviations. The accuracies for relevant experiments can be found in Figure 5. The optimal hyperparameters ρ in iKFAD and c in CD exhibit a wide range in magnitude across tasks indicating a strong dependence on gradient scales in each setting. This was not explored, but it could be remedied by normalizing gradients between training iterations.

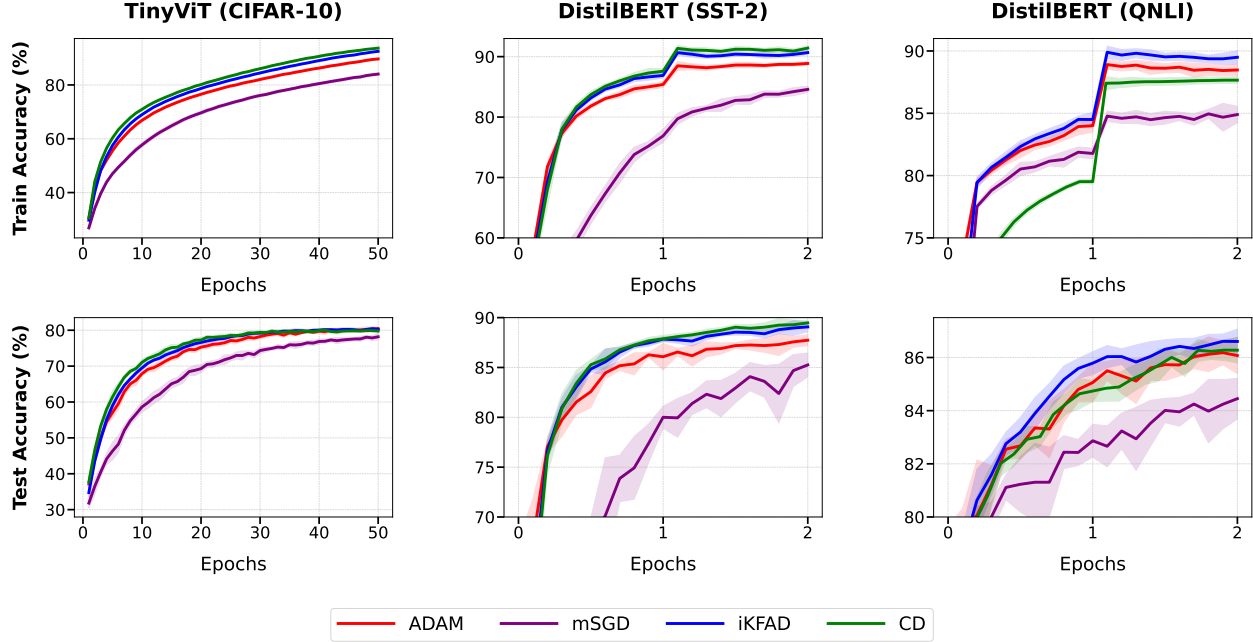


Figure 5: Corresponding training and test accuracies for the experiments in Figure 4. Standard deviations are included.

In Figure 6, we study the effect of removing the linear friction γ on the dynamics of iKFAD and CD. We observe that setting $\gamma = 0$ does not worsen performance, suggesting that the linear damping term is not essential in practice and can be removed to reduce the number of hyperparameters by one.

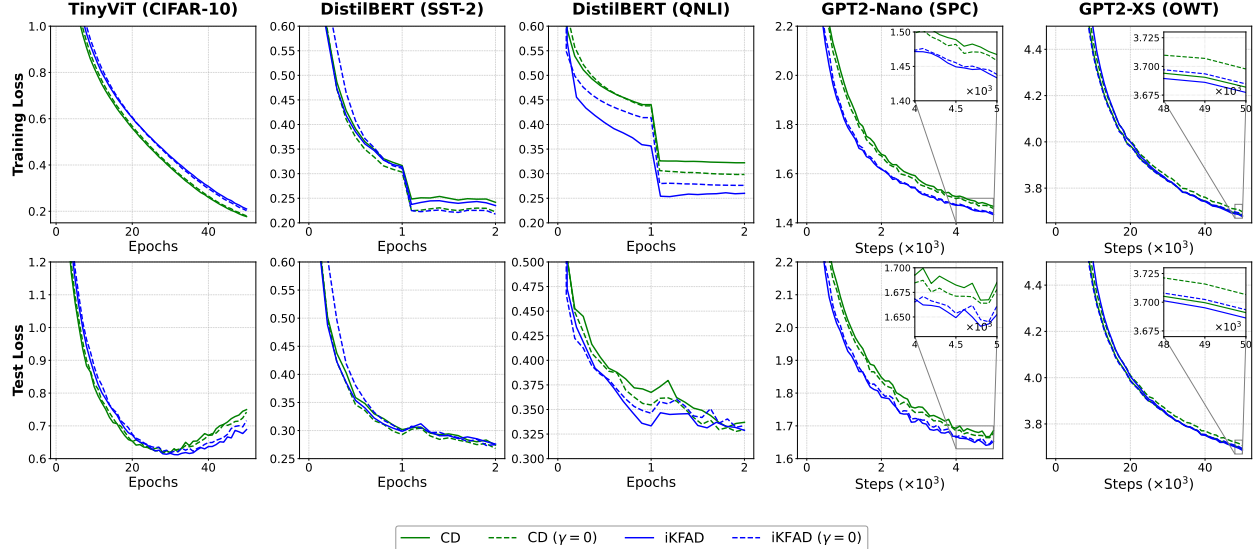


Figure 6: **Effect of removing linear damping.** Hyperparameter sweeps for CD and iKFAD comparing $\gamma = 0$ against $\gamma \in [10^{-6}, 10]$. Setting $\gamma = 0$, does not worsen performance, allowing us to eliminate γ as a hyperparameter.

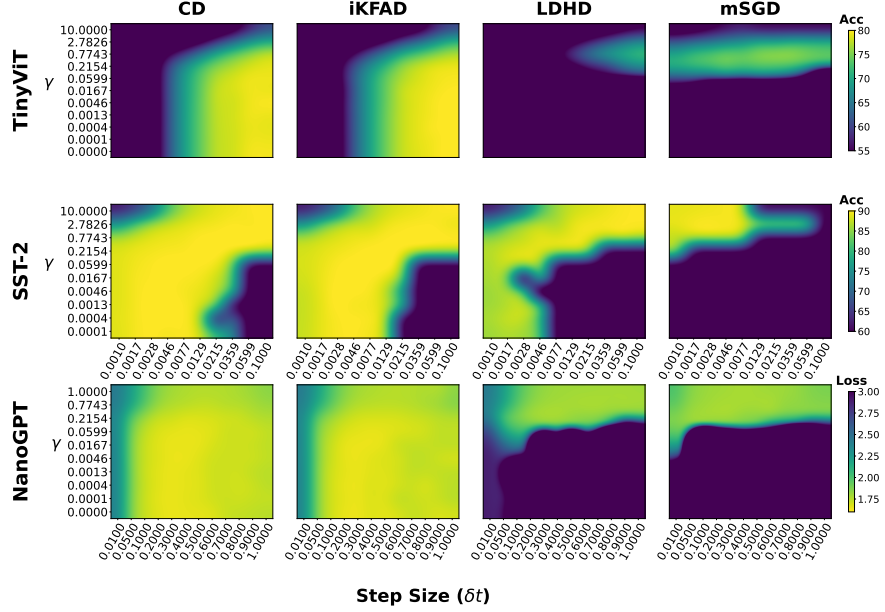


Figure 7: $\gamma - \delta t$ grid. Test accuracies/losses for iKFAD, CD, LDHD, and mSGD on various experiments as functions of learning rate δt and linear friction γ . Higher color intensity indicates better performance. γ for mSGD is obtained by the correspondence derived in Appendix A. LDHD uses splitting for discretization.

The best CD and iKFAD results from the current figure (either $\gamma = 0$ or $\gamma > 0$) were selected to present in Figure 4.

6.2 Ablation on linear damping.

Removing linear damping $\gamma = 0$.

To study the role of the linear damping term γ , we repeat the experiments in Figure 4 with $\gamma = 0$ and present the results in Figure 6. This isolates the effect of adaptive friction and cubic damping. We find that while CADAM tends not to perform very well without linear friction (see Appendix E Figure 11), CD and iKFAD maintain their good performance even when $\gamma = 0$. This is expected because after hyperparameter optimization in the $\gamma > 0$ setting, the optimal γ values were typically near the lower end of the search range for CD and iKFAD. Hence, we can set $\gamma = 0$, which reduces the hyperparameter count for both CD and iKFAD to two and three hyperparameters respectively (matching mSGD and Adam). We note that the hyperparameter search space for sweeps with $\gamma = 0$ searches over one dimension less than if we set $\gamma > 0$. This offers a possible explanation as to why $\gamma = 0$ sweeps arrive at a better hyperparameter configuration. The results of CADAM are presented in Appendix E. We observe that CADAM tends to rely more heavily on linear damping (see Figure 11) and Table 4 where optimal γ values corresponding to CADAM are significantly higher).

Varying $\gamma - \delta t$.

To assess the robustness of iKFAD and CD with respect to the learning rate δt and linear friction γ , we evaluated both optimizers across the NanoGPT (SPC), DistilBERT (SST2), and TinyViT (CIFAR-10) tasks. Note that while we vary γ and δt , the rest of the hyperparameters are kept fixed at some reasonable values (the best setting for each experiment from Section 6. We compare against mSGD and LDHD. For mSGD, we map γ to the momentum parameter μ using the correspondence derived in Appendix A. LDHD corresponds to the same continuous dynamics as mSGD, but while mSGD uses an Euler discretization, LDHD uses a splitting discretization. Figure 7 shows that iKFAD and CD maintain substantially higher robustness and accuracy over wide ranges of $(\gamma, \delta t)$ compared to mSGD and LDHD. Both iKFAD and CD also exhibit very similar behavior in terms of test metrics. This indicates that iKFAD is close to equilibrium $\dot{\xi} = 0$ for the majority of training. This is expected, as iKFAD and CD are closely related: in both methods the amount of damping depends on kinetic energy. In iKFAD, the adaptive friction variable ξ is an exponentially weighted average of past kinetic energies ($[p]^2$), so damping reflects a short history of the dynamics. In CD, the damping is instantaneous. The cubic term can be written as $-c[p]^2 \star p$, i.e., the damping coefficient scales with the current kinetic energy p^2 . We note that both optimizers remain effective even for very small γ , demonstrating that their adaptive friction and cubic damping mechanisms can compensate for minimal linear damping. We also observe that the optimal hyperparameter for

CD $c \approx \frac{1}{\alpha\rho}$ is obtained in some of the experiments (e.g NanoGPT), which also reflects the aforementioned connection between the two methods. As a side note, mSGD and LDHD share the same underlying continuous dynamics, but their stability regions differ under the discretizations used, as demonstrated in Figure 7.

7 Conclusion and future work

In this work, we introduce Individual Kinetic Friction Adaptive Descent (iKFAD), Cubically Damped mSGD (CD), and Cubically Damped Adam (CADAM), a family of optimizers motivated by a continuous-time view of momentum as friction that regulates kinetic energy. By making the connection between adaptive friction and cubic damping explicit, we obtain a simple set of dynamics that improve stability and can accelerate convergence in practice. We also prove exponential decay for both the continuous-time systems and their discrete-time schemes. Across image and language benchmarks, our methods are more robust to learning-rate choice, often generalize better, and achieve test performance that is competitive with, or better than, Adam. In particular, iKFAD and CD bridge much of the Adam–mSGD gap in language modeling without relying on per-parameter learning rates. Notably, CD (with $\gamma = 0$) achieves this while keeping the same memory footprint as mSGD.

Limitations and Future Work. The computational cost of hyperparameter tuning limited our study to at most 80 trials per experiment. Also, since our benchmarks were limited to models under 100M parameters, evaluating these schemes on large-scale LLMs remains future work. On the theory side, we have not yet obtained exponential convergence guarantees for CADAM similar to those proved for iKFAD and CD.

Acknowledgements

This research was supported by the MAC-MIGS Centre for Doctoral Training. This work of G.S. is supported by Hi! PARIS and ANR/France 2030 program (ANR-23-IACL-0005). We would like to thank Cameron Barker for his useful insights on configurations for language model training.

References

- [1] A. Babister. Non-linear differential equations having both cubic damping and stiffness. Technical Report 7601, University of Glasgow, 1976. Department of Aeronautics and Fluid Mechanics.
- [2] Dami Choi, Christopher J. Shallue, Zachary Nado, Jaehoon Lee, Chris J. Maddison, and George E. Dahl. On empirical comparisons of optimizers for deep learning, 2020.
- [3] Anna Choromanska, Mikael Henaff, Michael Mathieu, Gérard Ben Ben Arous, and Yann LeCun. The Loss Surfaces of Multilayer Networks. In Guy Lebanon and S. V. N. Vishwanathan, editors, *Proceedings of the Eighteenth International Conference on Artificial Intelligence and Statistics*, volume 38 of *Proceedings of Machine Learning Research*, pages 192–204, San Diego, California, USA, 2015. PMLR.
- [4] André Belotto Da Silva and Maxime Gazeau. A general system of differential equations to model first-order adaptive algorithms. *The Journal of Machine Learning Research*, 21(1):5072–5113, 2020.
- [5] Nan Ding, Youhan Fang, Ryan Babbush, Changyou Chen, Robert D. Skeel, and Hartmut Neven. Bayesian sampling using stochastic gradient thermostats. In Z. Ghahramani, M. Welling, C. Cortes, N. Lawrence, and K.Q. Weinberger, editors, *Advances in Neural Information Processing Systems*, volume 27. Curran Associates, Inc., 2014.
- [6] Paul Dobson, Jesus Maria Sanz-Serna, and Konstantinos Zygalakis. On the connections between optimization algorithms, lyapunov functions, and differential equations: theory and insights. *arXiv preprint arXiv:2305.08658*, 2023.
- [7] X. Gao, M. Gurbuzbalaban, and L. Zhu. Global convergence of stochastic gradient hamiltonian monte carlo for non-convex stochastic optimization: Non-asymptotic performance bounds and momentum-based acceleration, 2018.
- [8] Aikaterini Karoni. *Higher-order damping mechanisms with applications in optimisation and machine learning*. PhD thesis, The University of Edinburgh, 2024.
- [9] Aikaterini Karoni, Benedict Leimkuhler, and Gabriel Stoltz. Friction-adaptive descent: A family of dynamics-based optimization methods. *Journal of Computational Dynamics*, 2023.

[10] Andrej Karpathy. nanogpt: The simplest, fastest repository for training/finetuning medium-sized gpts. <https://github.com/karpathy/nanoGPT>, 2022. Accessed: 2026-01-22.

[11] Diederik P. Kingma and Jimmy Ba. Adam: A method for stochastic optimization. In Yoshua Bengio and Yann LeCun, editors, *3rd International Conference on Learning Representations, ICLR 2015, San Diego, CA, USA, May 7-9, 2015, Conference Track Proceedings*, 2015.

[12] Alex Krizhevsky, Geoffrey Hinton, et al. Learning multiple layers of features from tiny images. Technical report, University of Toronto, 2009.

[13] Frederik Kunstner, Jacques Chen, Jonathan Wilder Lavington, and Mark Schmidt. Noise is not the main factor behind the gap between sgd and adam on transformers, but sign descent might be. *arXiv preprint arXiv:2304.13960*, 2023.

[14] Benedict Leimkuhler and Sebastian Reich. *Simulating Hamiltonian Dynamics*. Cambridge Monographs on Applied and Computational Mathematics. Cambridge University Press, 2005.

[15] Hao Li, Zheng Xu, Gavin Taylor, Christoph Studer, and Tom Goldstein. Visualizing the loss landscape of neural nets. *Advances in neural information processing systems*, 31, 2018.

[16] C.J. Maddison, D. Paulin, Y.W. Teh, B. O'Donoghue, and A. Doucet. Hamiltonian descent methods. *arXiv preprint*, 1809.05042, 2018.

[17] Martin Marek, Sanae Lotfi, Aditya Somasundaram, Andrew Gordon Wilson, and Micah Goldblum. Small batch size training for language models: When vanilla SGD works, and why gradient accumulation is wasteful. In *The Thirty-ninth Annual Conference on Neural Information Processing Systems*, 2025.

[18] J.C. Mattingly, A.M. Stuart, and D.J. Higham. Ergodicity for SDEs and approximations: locally Lipschitz vector fields and degenerate noise. *Stochastic Processes and their Applications*, 101(2):185–232, 2002.

[19] Céline Moucer, Adrien Taylor, and Francis Bach. A systematic approach to Lyapunov analyses of continuous-time models in convex optimization. *SIAM Journal on Optimization*, 33(3):1558–1586, 2023.

[20] Yurii Nesterov. A method of solving a convex programming problem with convergence rate $o(\frac{1}{k^2})$. *Doklady Akademii Nauk SSSR*, 269(3):543, 1983.

[21] Yurii Nesterov. *Introductory lectures on convex optimization: A basic course*, volume 87. Springer Science & Business Media, 2013.

[22] Brendan O'Donoghue and Emmanuel Candès. Adaptive restart for accelerated gradient schemes. *Found. Comput. Math.*, 15(3):715–732, 2015.

[23] N. Panananda, N.S. Ferguson, and T.P. Waters. The effect of cubic damping in an automotive vehicle suspension model. In *Computational Modelling and Analysis of Vehicle Body Noise and Vibration*, 2012.

[24] Z. K. Peng, Z. Q. Lang, X. J. Jing, S. A. Billings, G. R. Tomlinson, and L. Z. Guo. The transmissibility of vibration isolators with a nonlinear antisymmetric damping characteristic. *Journal of Vibration and Acoustics*, 132(1):014501, 01 2010.

[25] B. T. Poljak. Some methods of speeding up the convergence of iterative methods. *Ž. Vyčisl. Mat i Mat. Fiz.*, 4:791–803, 1964.

[26] Xiaocheng Shang, Zhanxing Zhu, Benedict Leimkuhler, and Amos J Storkey. Covariance-controlled adaptive langevin thermostat for large-scale bayesian sampling. In C. Cortes, N. Lawrence, D. Lee, M. Sugiyama, and R. Garnett, editors, *Advances in Neural Information Processing Systems*, volume 28. Curran Associates, Inc., 2015.

[27] Luke Shaw and Peter A Whalley. Randomised splitting methods and stochastic gradient descent. *arXiv preprint arXiv:2504.04274*, 2025.

[28] U. Simsekli, L. Zhu, Y.-W. Teh, and M. Gurbuzbalaban. Fractional underdamped langevin dynamics: Retargeting sgd with momentum under heavy-tailed gradient noise. In *International conference on machine learning*, pages 8970–8980. PMLR, 2020.

[29] Weijie Su, Stephen Boyd, and Emmanuel J. Candès. A differential equation for modeling Nesterov's accelerated gradient method: theory and insights. *J. Mach. Learn. Res.*, 17:Paper No. 153, 43, 2016.

[30] Ilya Sutskever, James Martens, George Dahl, and Geoffrey Hinton. On the importance of initialization and momentum in deep learning. In *International conference on machine learning*, pages 1139–1147. PMLR, 2013.

[31] Akiyoshi Tomihari and Issei Sato. Understanding why adam outperforms sgd: Gradient heterogeneity in transformers. *arXiv preprint arXiv:2502.00213*, 2025.

- [32] Alex Wang, Amanpreet Singh, Julian Michael, Felix Hill, Omer Levy, and Samuel R Bowman. Glue: A multi-task benchmark and analysis platform for natural language understanding. *arXiv preprint arXiv:1804.07461*, 2018.
- [33] Kan Wu, Jinnian Zhang, Houwen Peng, Mengchen Liu, Bin Xiao, Jianlong Fu, and Lu Yuan. Tinyvit: Fast pretraining distillation for small vision transformers. In *European conference on computer vision (ECCV)*, 2022.
- [34] Jingzhao Zhang, Sai Praneeth Karimireddy, Andreas Veit, Seungyeon Kim, Sashank Reddi, Sanjiv Kumar, and Suvrit Sra. Why are adaptive methods good for attention models? *Advances in Neural Information Processing Systems*, 33:15383–15393, 2020.
- [35] Yushun Zhang, Congliang Chen, Tian Ding, Ziniu Li, Ruoyu Sun, and Zhi-Quan Luo. Why transformers need adam: A hessian perspective. In A. Globerson, L. Mackey, D. Belgrave, A. Fan, U. Paquet, J. Tomczak, and C. Zhang, editors, *Advances in Neural Information Processing Systems*, volume 37, pages 131786–131823. Curran Associates, Inc., 2024.
- [36] YP. Zhu and Z.Q. Lang. Beneficial effects of antisymmetric nonlinear damping with application to energy harvesting and vibration isolation under general inputs. *Nonlinear Dynamics*, 108:2917–2933, 2022.

A Equivalence between mSGD and LDHD

In this section we will show how the mSGD discrete equations (1a), (1b) can be obtained as an Euler discretisation of linearly dissipative Hamiltonian dynamics (LDHD) (2a), (2b). We start with the system of ODEs corresponding to LDHD

$$\begin{aligned}\dot{x} &= p, \\ \dot{p} &= -\nabla f(x) - \gamma p.\end{aligned}$$

Applying Euler discretization, with time step δt , we obtain

$$\begin{aligned}p_{n+1} &= p_n + \delta t(-\nabla f(x_n) - \gamma p_n) &\implies p_{n+1} &= (1 - \delta t \gamma)p_n - \delta t \nabla f(x_n) \\ x_{n+1} &= x_n + \delta t p_{n+1} &x_{n+1} &= x_n + \delta t p_{n+1}\end{aligned}$$

Dividing the momentum equation by the learning rate δt , we obtain

$$\begin{aligned}\frac{p_{n+1}}{\delta t} &= (1 - \delta t \gamma) \frac{p_n}{\delta t} - \nabla f(x_n), &\stackrel{\tilde{p} = p/\delta t}{\implies} \tilde{p}_{n+1} &= (1 - \delta t \gamma) \tilde{p}_n - \nabla f(x_n), \\ x_{n+1} &= x_n + \delta t^2 \frac{p_{n+1}}{\delta t}, &x_{n+1} &= x_n + \delta t^2 \tilde{p}_{n+1}.\end{aligned}$$

Finally, after setting $\tilde{\delta t} = \delta t^2$ and $\mu = (1 - \gamma \sqrt{\tilde{\delta t}})$, we have

$$\begin{aligned}\tilde{p}_{n+1} &= (1 - \gamma \sqrt{\tilde{\delta t}}) \tilde{p}_n - \nabla f(x_n), &\stackrel{\bar{p} = -\tilde{p}}{\implies} \bar{p}_{n+1} &= \mu \bar{p}_n + \nabla f(x_n), \\ x_{n+1} &= x_n + \tilde{\delta t} \tilde{p}_{n+1}, &x_{n+1} &= x_n - \tilde{\delta t} \bar{p}_{n+1},\end{aligned}$$

which is exactly the system of discrete momentum gradient descent equations (1a), (1b). Although this equivalence is correct, there are pairings $(\gamma, \delta t)$ for which it would be invalid because $\mu > 0$ i.e., $\gamma \cdot \delta t > 1$.

B Analytical Updates in Splitting

To derive practical discrete-time algorithms from the continuous-time dynamics, we employ an operator-splitting approach. The key idea is to decompose a complex system of ordinary differential equations (ODEs) into a sum of simpler sub-dynamics, each of which can be solved exactly in closed form. Rather than integrating the full coupled system at once, which typically admits no analytical solution, we sequentially apply the exact flows of these sub-systems over short time intervals and compose them to obtain a single update step.

Table 2: Splitting of ODE dynamics for iKFAD, CD, and CADAM.

iKFAD	$\begin{pmatrix} \dot{x} \\ \dot{p} \\ \dot{\xi} \end{pmatrix} = \underbrace{\begin{pmatrix} p \\ 0 \\ 0 \end{pmatrix}}_{\text{A}} + \underbrace{\begin{pmatrix} 0 \\ -\nabla f(x) \\ 0 \end{pmatrix}}_{\text{B}} + \underbrace{\begin{pmatrix} 0 \\ -\xi \star p \\ \frac{[p]^2}{\rho} \end{pmatrix}}_{\text{C}} + \underbrace{\begin{pmatrix} 0 \\ -\gamma p \\ -\alpha \xi \end{pmatrix}}_{\text{D}}$
CD	$\begin{pmatrix} \dot{x} \\ \dot{p} \end{pmatrix} = \underbrace{\begin{pmatrix} p \\ 0 \end{pmatrix}}_{\text{A}} + \underbrace{\begin{pmatrix} 0 \\ -\nabla f(x) \end{pmatrix}}_{\text{B}} + \underbrace{\begin{pmatrix} 0 \\ -c[p]^3 \end{pmatrix}}_{\text{C}} + \underbrace{\begin{pmatrix} 0 \\ -\gamma p \end{pmatrix}}_{\text{D'}}$
CADAM	$\begin{pmatrix} \dot{x} \\ \dot{p} \\ \dot{\zeta} \end{pmatrix} = \underbrace{\begin{pmatrix} \frac{p}{\sqrt{\zeta+\epsilon}} \\ 0 \\ 0 \end{pmatrix}}_{\text{A'}} + \underbrace{\begin{pmatrix} 0 \\ -\nabla f(x) \\ 0 \end{pmatrix}}_{\text{B}} + \underbrace{\begin{pmatrix} 0 \\ -c[p]^3 \\ 0 \end{pmatrix}}_{\text{C'}} + \underbrace{\begin{pmatrix} 0 \\ -\gamma p \\ 0 \end{pmatrix}}_{\text{D'}} + \underbrace{\begin{pmatrix} 0 \\ 0 \\ [\nabla f(x)]^2 - \alpha \zeta \end{pmatrix}}_{\text{E}}$

Concretely, consider an ODE of the form $\dot{z} = \sum_k F_k(z)$, where each vector field F_k represents a distinct physical or algorithmic effect (e.g., transport, gradient forcing, damping, or adaptive scaling). Operator splitting replaces the exact flow of the full system over a time step δt by a composition of flows induced by each F_k individually. When each sub-system $\dot{z} = F_k(z)$ is analytically solvable, this yields explicit and stable update rules without requiring numerical ODE solvers. For more information about splitting methods, please refer to [14].

In our setting, the dynamics of iKFAD, CD, and CADAM naturally decompose into interpretable components such as position transport, gradient descent, nonlinear momentum damping, and auxiliary-state adaptation. Table 2 lists the resulting decomposition into sub-operators (labeled A–E), while Table 3 reports the corresponding exact solutions over a time interval δt . The discrete-time optimizers studied in the main text are obtained by composing these analytical updates in a prescribed order, yielding schemes that faithfully reflect the underlying continuous-time structure while remaining fully explicit.

The discrete-time optimizers are constructed using first-order Lie-Trotter operator splitting. Specifically, for iKFAD, we employ the CDBA composition, while CD follows a C'D'BA sequence. CADAM utilizes a C'D'BAE ordering, where E represents the update for the second-moment estimate. While higher-order symmetric splittings (such as the second-order Strang splitting) exist, we find that these first-order compositions are sufficient to preserve the qualitative dissipative structure of the continuous dynamics while maintaining a low computational cost per iteration. In each case, the full update $z_{n+1} = \Phi_{\delta t}(z_n)$ is obtained by the sequential application of the analytical sub-flows detailed in Table 3.

Table 3: Analytical updates for unique splitting steps.

Step	Analytical update
A	$x_{n+1} = x_n + \delta t p_n$
A'	$x_{n+1} = x_n + \delta t \frac{p_n}{\sqrt{\zeta_n + \epsilon}}$
B	$p_{n+1} = p_n - \delta t \nabla f(x_n)$
C	$p_{n+1} = e^{-\Xi_n \delta t} p_n,$ $\tilde{\xi}_{n+1} = \sqrt{[\xi_n]^2 + \frac{(I - e^{-2\Xi_n \delta t})}{\rho} [p_n]^2}$
C'	$p_{n+1} = \frac{p_n}{\sqrt{1 + 2c[p_n]^2 \delta t}}$
D	$p_{n+1} = e^{-\gamma \delta t} p_n,$ $\xi_{n+1} = e^{-\alpha \delta t} \tilde{\xi}_{n+1}$
D'	$p_{n+1} = e^{-\gamma \delta t} p_n$
E	$\zeta_{n+1} = e^{-\alpha \delta t} \zeta_n + \frac{(1 - e^{-\alpha \delta t})}{\alpha} [\nabla f(x_n)]^2$

C Comparison of known momentum schedules to our adaptive one

Both [30] and [20] propose gradually increasing the momentum parameter μ for non-strongly-convex functions, which is typical of neural network loss landscapes. The schedules are given by

$$\begin{aligned}\mu_t &= \min\left(1 - 2^{-1-\log_2(\lfloor \frac{t}{250} \rfloor + 1)}, \mu_{\max}\right), \\ \mu_t &= 1 - \frac{3}{t + 5},\end{aligned}\tag{13}$$

respectively. iKFAD naturally reproduces this behaviour. Since an increase in μ corresponds to a decrease in γ ((3)), the gradual reduction of friction observed in Figure 8 aligns with the progressive momentum increase proposed in [20] and [30]. As optimization progresses toward equilibrium $(\nabla f(x^*), p^*) = (0, 0)$, the system's kinetic energy decays, leading to a corresponding decrease in the adaptive friction ξ . Intuitively, higher friction (lower momentum) at the beginning of training allows careful exploration of the loss landscape, while lower friction later facilitates traversal of flat regions and local minima. Unlike static or monotonic schedules [30, 20], our thermostated mechanism adapts friction dynamically and individually per parameter, preventing excessive buildup of momentum.

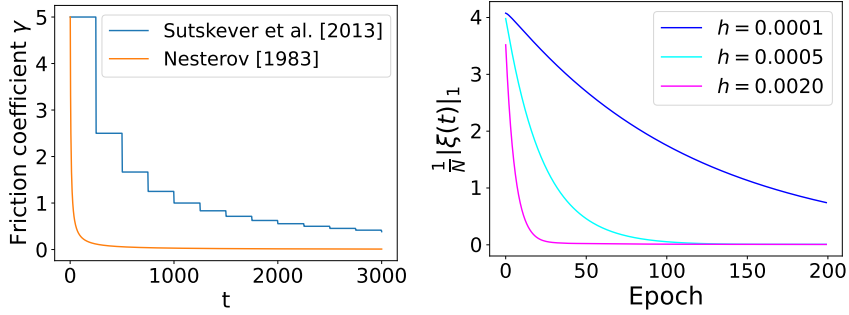


Figure 8: Left: Friction schedules corresponding to (13) via the mapping in (3) ($h = 0.01$). Right: Mean L^1 -norm of the adaptive friction ξ in iKFAD (with $\gamma = 0$) during ResNet18 training on FashionMNIST for three learning rates. The decreasing trend of ξ mirrors the momentum annealing behaviour in classical schedules.

D ResNet-18 on CIFAR-10 Results

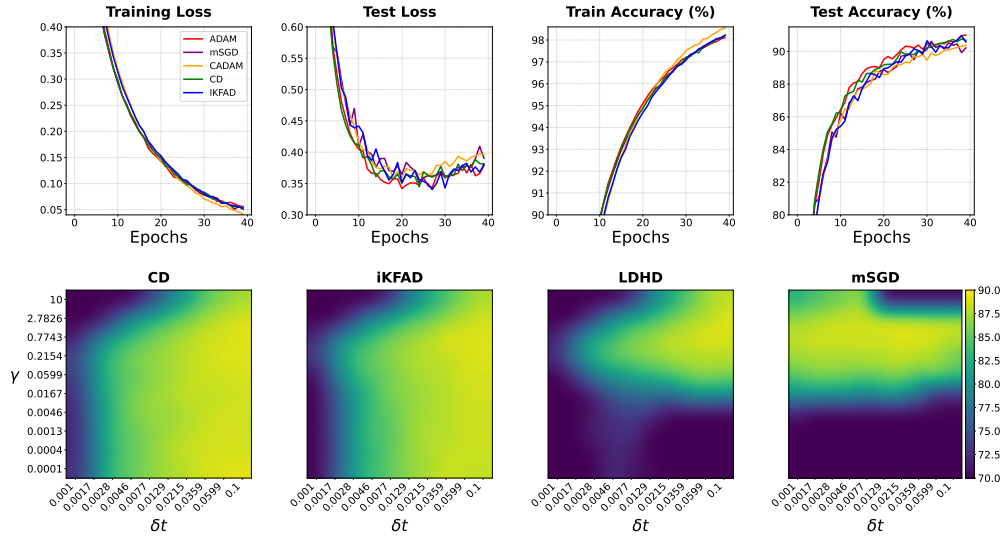


Figure 9: Complete Results on ResNet-18. First row has train + test accuracy and losses. Second row is a grid search on linear damping and learning rate.

For ResNet-18, we train on CIFAR-10 we choose a batch size of 128. After hyperparameter tuning, the performance of all optimizers is comparable. This is a well-documented result [2] where after hyperparameter tuning, most standard optimizers on ResNet or VGG architectures will perform roughly the same. On the other hand, iKFAD and CD display greater robustness to hyperparameter variations as highlighted in the second row by the $\gamma - \delta t$ grid of test accuracies. It is also interesting to see that CADAM achieves a lower training loss but a higher test loss. This might indicate that CADAM is more prone to overfitting. Perhaps it is due to the lack of bias correction in the CADAM dynamics that is there in Adam. It is also worth commenting on the differences between LDHD and mSGD. They have the same underlying continuous dynamics but only differ in the way they are discretized. It would appear that they are mostly stable in the same regions, but mSGD does not converge in the high $(\gamma, \delta t)$ cases.

E CADAM Results

We present the complete experimental results in this section, including full CADAM loss curves and corresponding confidence intervals. As a preliminary observation, CADAM maintains three optimizer state variables, mirroring Adam, but additionally introduces one extra hyperparameter. Despite this similarity, its behavior differs substantially in practice. As shown in Fig. 11, CADAM fails to operate reliably in the absence of linear damping. When linear damping is removed and optimization relies solely on cubic damping, we observe a dramatic degradation in performance across all settings. A plausible explanation for this behavior lies in the role of the linear damping term in approximating second-order curvature information. In particular, the linear damping effectively serves as a diagonal approximation to the local Fisher information matrix, thereby providing a stabilizing preconditioning effect similar in spirit to Adam’s adaptive learning rates. When only cubic damping is employed, this approximation is lost, and the optimizer no longer benefits from a meaningful estimate of local curvature. As a result, parameter updates become poorly scaled, leading to instability and significantly worse convergence behavior. Furthermore, CADAM does not incorporate bias correction for its moment estimates. This omission is especially detrimental during the early stages of training, where biased moment estimates can severely distort update magnitudes. Empirically, this issue manifests clearly in our experiments: CADAM performs poorly across all evaluated tasks, and in the GPT2-Nano setting the training loss diverges entirely. To accommodate these unstable runs, we rescale the axes of the plots to include results corresponding to $\gamma = 0$. When linear damping is enabled, as shown in Fig. 10, CADAM exhibits markedly improved stability and can occasionally achieve performance comparable to Adam. However, even in this regime, CADAM is generally inferior to Adam across most tasks. The sole exception is the DistilBERT model trained on SST-2, where CADAM marginally outperforms Adam. Overall, these results suggest that linear damping and its implicit approximation of diagonal Fisher information, is critical to CADAM’s viability, yet insufficient to consistently surpass established adaptive optimizers such as Adam.

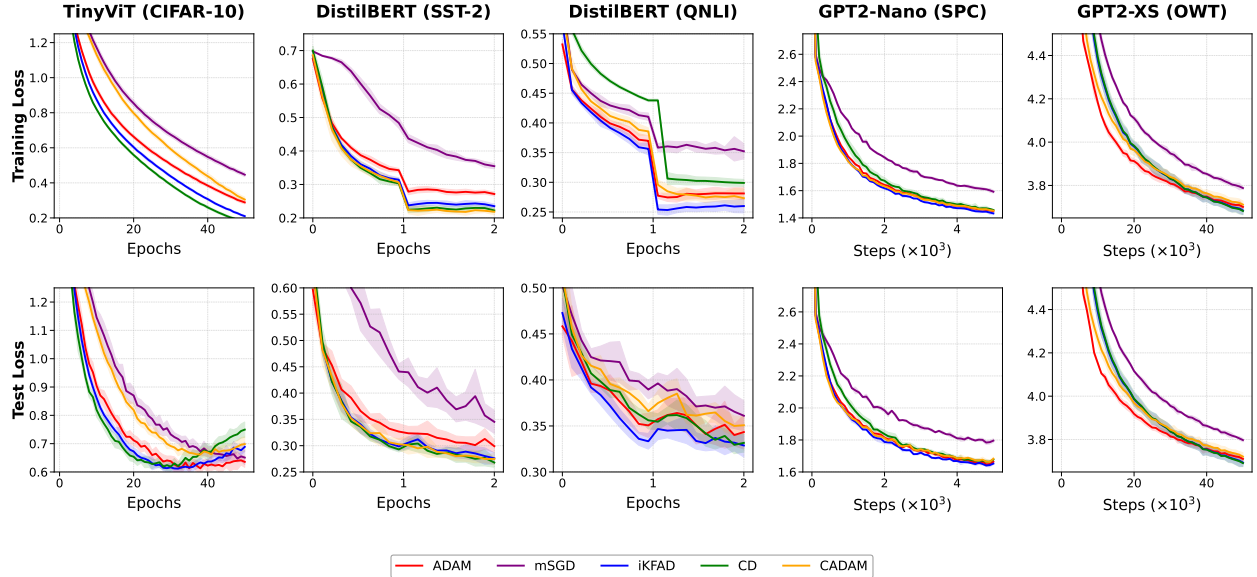


Figure 10: **Complete results of losses including CADAM.** This includes standard deviations. CADAM (yellow) performs competitively to Adam in some cases. However, more often than not, the performance of CADAM is slightly worse. Despite having the same number of optimizer states and hyperparameters as Adam, with the advantage of per-parameter adaptive learning rates, CADAM still does not perform as well as iKFAD and CD.

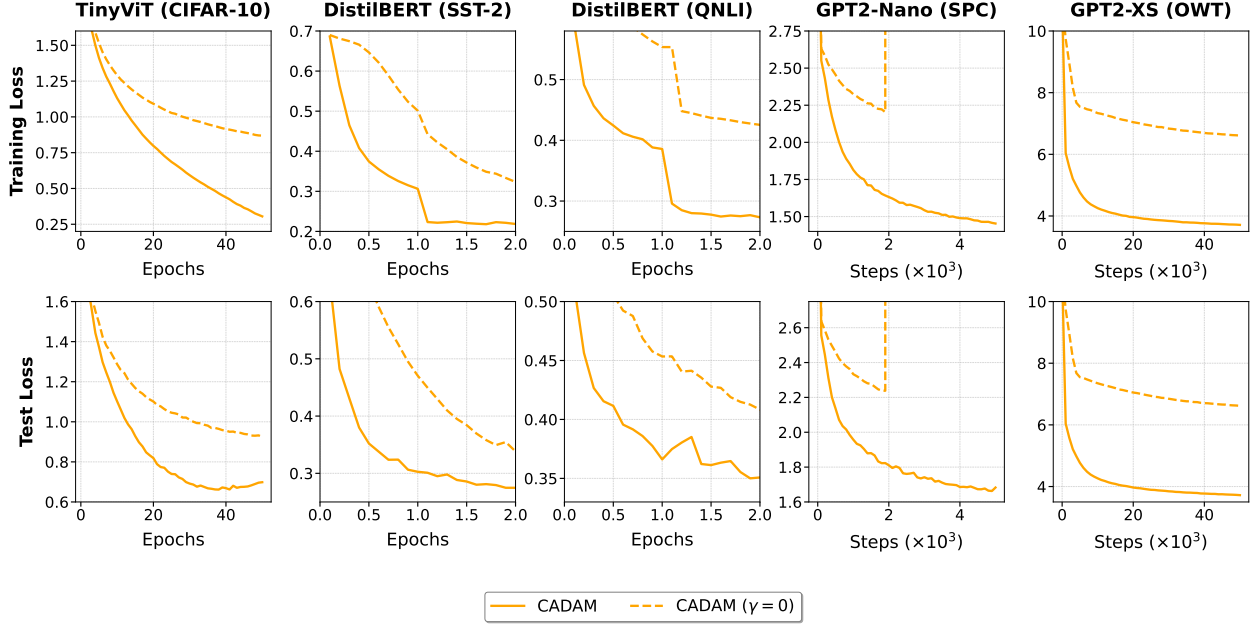


Figure 11: **CADAM when $\gamma = 0$.** We conducted a hyperparameter sweep when $\gamma = 0$ and when $\gamma \in [1e-6, 10]$ for CADAM. This is the same experiment as done in Figure 6, but for CADAM. It is clear that CADAM relies heavily on linear damping. This implies that the cubic damping mechanism is not as helpful when per-parameter learning rates are already available. The scale of the plots were adjusted to include the curves of CADAM when $\gamma = 0$. In fact, relative to Figure 4, the drop in performance when removing linear damping from CADAM is quite dramatic.

F Hyperparameter values for Optuna searches

Across all models, we observed a dramatic variance in the optimal scales for the ρ (iKFAD) and c (CD) hyperparameters. This variance likely stems from the fact that these coefficients are inherently coupled to the scale of gradient norms at equilibrium. While normalizing gradients between iterations could potentially unify these hyperparameter scales, we leave this exploration for future work. Experimental configurations:

- **ResNet18-CIFAR-10:** batch size 128, 40 epochs, $\gamma \in [10^{-9}, 10]$, $(\rho, c, \alpha) \in [10^{-9}, 10^{10}]$. $h \in [10^{-6}, 10^{-2}]$ for CADAM and $h \in [10^{-6}, 10^{-1}]$ for iKFAD and CD. The ranges here are quite vast as this was the very first experiment.
- **TinyViT - CIFAR-10:** batch size 128, 50 epochs. $\gamma \in [10^{-5}, 10]$, $\rho \in [10^{-8}, 10]$, $c \in [10^4, 10^{10}]$. $h \in [10^{-6}, 10^{-2}]$ for CADAM and $h \in [10^{-4}, 3 \times 10^{-1}]$ for iKFAD and CD.
- **DistilBERT - SST-2:** batch size 16, 2 epochs, $\gamma \in [10^{-6}, 1]$ for CADAM/iKFAD and $\gamma = 0$ for CD, $\rho \in [10^{-8}, 10]$, $\alpha \in [0.001, 1]$.
- **DistilBERT - QNLI:** batch size 16, 2 epochs, $\gamma \in [10^{-6}, 1]$ for CADAM/iKFAD and $\gamma = 0$ for CD, $c \in [0.01, 10^{13}]$, $\alpha \in [0.001, 10]$, $\rho \in [10^{-8}, 10]$.
- **GPT2-Nano - Shakespeare:** batch size 16, 5000 steps. $\gamma \in [10^{-5}, 10]$, $h \in [10^{-5}, 5 \times 10^{-1}]$ for CD/iKFAD and $h \in [10^{-6}, 10^{-2}]$ for CADAM, $c \in [10^{-1}, 10^6]$, $\alpha \in [10^{-3}, 10]$ for CADAM and $\alpha \in [10^{-5}, 10]$ for iKFAD. $\rho \in [10^{-8}, 10]$
- **GPT2-XS - OpenWebText:** batch size 16, 50000 steps. $h \in [10^{-6}, 10^{-2}]$ for CADAM and $h \in [10^{-4}, 10^{-1}]$ for CD/iKFAD. $\gamma \in [10^{-5}, 10]$. $\alpha \in [10^{-3}, 1]$. $c \in [10^4, 10^{10}]$. $\rho \in [10^{-8}, 10]$.

For all experiments, Adam and mSGD were swept over: $h \in [10^{-6}, 10^{-2}]$ for Adam and $h \in [10^{-6}, 10^{-1}]$ for mSGD and $\mu \in [0.5, 0.99]$, $\beta_1 \in [0.85, 0.999]$, $\beta_2 \in [0.85, 0.999]$.

Table 4: Optimized hyperparameters for all loss curves in Figure 4.

	δt	γ	α	ρ	c	β_1	β_2	μ
ResNet-18								
iKFAD	0.0973	0.40	0.402	1.87	-	-	-	-
CD	0.0448	0.17	-	-	56814.47	-	-	-
CADAM	0.0037	3.55	0.005	-	82552.90	-	-	-
mSGD	0.0260	-	-	-	-	-	-	0.86
Adam	0.0008	-	-	-	-	0.97	0.99	-
TinyViT								
iKFAD	0.08991	0.04537	0.10110	6.29×10^{-6}	-	-	-	-
CD	0.19983	0.00221	-	-	6.55×10^5	-	-	-
CADAM	0.00197	4.46870	24314309	-	0.91377	-	-	-
mSGD	0.02133	-	-	-	-	-	-	0.87439
Adam	0.00055	-	-	-	-	0.86082	0.88521	-
SST-2 (Pretrain)								
iKFAD	0.02704	1.28×10^{-6}	0.0465	3.61×10^{-7}	-	-	-	-
CD	0.0363	0	-	-	9.78×10^6	-	-	-
CADAM	0.00035	9.2188	0.03233	-	0.0237	-	-	-
mSGD	0.00237	-	-	-	-	-	-	0.8335
Adam	3.82×10^{-5}	-	-	-	-	0.9187	0.98254	-
QNLI (Finetune)								
iKFAD	0.0413	1.36×10^{-8}	2.80	6.71	-	-	-	-
CD	0.03144	0	-	-	1.90×10^8	-	-	-
CADAM	0.0002	9.66	0.0026	-	22754.57	-	-	-
mSGD	0.0015	-	-	-	-	-	-	0.895
Adam	3.52×10^{-5}	-	-	-	-	0.855	0.933	-
GPT2-XS (OWT)								
iKFAD	0.09956	0.	0.04756	1.04×10^{-5}	-	-	-	-
CD	0.09975	0.00138	-	-	1.43×10^6	-	-	-
CADAM	0.00678	7.53239	0.44020	-	3.11×10^6	-	-	-
mSGD	0.05362	-	-	-	-	-	-	0.95277
Adam	0.00065	-	-	-	-	0.89447	0.99454	-
NanoGPT (Shakespeare)								
iKFAD	0.39055	2.58×10^{-5}	0.03474	0.00017	-	-	-	-
CD	0.42614	0	-	-	1.95×10^5	-	-	-
CADAM	0.00828	9.47376	8.82877	-	0.95201	-	-	-
mSGD	0.09791	-	-	-	-	-	-	0.90054
Adam	0.00168	-	-	-	-	0.88757	0.92653	-

G Ablation of $\gamma = 0$

For ablations of setting $\gamma = 0$, we used all the same hyperparameter search ranges as in the previous section but just changed $\gamma = 0$. There were some curves with $\gamma = 0$ that ended up doing better than $\gamma > 0$. We ended up choosing those as the "overall" best hyperparameters when presenting them in Figure 4. In Table 5, the left column denotes hyperparameters when $\gamma > 0$ while the right column is when $\gamma = 0$ so the γ column is omitted. We see that the other values are of roughly the same scale without too much difference for CD/iKFAD. However, note that the search space for a Bayesian hyperparameter search is one dimension smaller when we set $\gamma = 0$ which may explain why better results might be seen for that in some cases.

Table 5: Comparison of optimal hyperparameters. Left: Unconstrained ($\gamma > 0$). Right: Constrained ($\gamma = 0$). Note: The ρ/c column denotes ρ for iKFAD and c for CD/CADAM.

Dataset	Method	Unconstrained ($\gamma > 0$)				Constrained ($\gamma = 0$)		
		δt	γ	α	ρ/c	δt	α	ρ/c
TinyViT	CD	0.200	0.0022	—	6.55×10^5	0.117	—	5.35×10^5
	iKFAD	0.090	0.045	0.101	6.29×10^{-6}	0.073	0.090	1.26×10^{-5}
	CADAM	0.0020	4.47	0.914	2.43×10^7	8.17×10^{-4}	0.173	8.84×10^9
SST-2	CD	0.0422	0.052	—	3.34×10^7	0.0363	—	9.78×10^6
	iKFAD	0.0270	1.28×10^{-6}	0.047	3.61×10^{-7}	0.0165	0.057	9.89×10^{-6}
	CADAM	3.49×10^{-4}	9.22	0.032	0.024	3.39×10^{-5}	0.021	3.39×10^5
QNLI	CD	0.0789	2.78	—	1.12×10^8	0.0314	—	1.90×10^8
	iKFAD	0.0413	1.36×10^{-8}	2.80	6.71×10^{-9}	0.0448	0.0017	2.77×10^{-7}
	CADAM	1.60×10^{-4}	9.66	0.0026	2.28×10^4	1.74×10^{-5}	0.033	1.52×10^7
GPT2-XS	CD	0.0997	0.0014	—	1.43×10^6	0.0990	—	1.37×10^6
	iKFAD	0.0763	0.0009	0.6737	1.3857×10^{-6}	0.0996	0.0476	1.0429×10^{-5}
	CADAM	0.0068	7.53	0.440	3.11×10^6	1.32×10^{-5}	0.491	1.43×10^8
NanoGPT	CD	0.499	0.0038	—	1.87×10^5	0.426	—	1.95×10^5
	iKFAD	0.391	2.58×10^{-5}	0.035	1.71×10^{-4}	0.494	2.20	4.55×10^{-6}
	CADAM	0.0083	9.47	8.83	0.952	0.0052	0.012	7.02×10^5

H iKFAD Convergence Analysis

This section establishes the convergence properties of the proposed iKFAD optimizer. We focus our analysis on strictly convex objective functions (specifically C^2 functions with bounded Hessian) to provide stability guarantees. We first prove that the continuous-time iKFAD dynamics converges at an exponential rate to the global minimum. We then show that this geometric convergence rate is preserved in a discrete-time setting, provided the step size δt is sufficiently small.

H.1 Dynamical properties of iKFAD

Equation 6c reads $\dot{\xi} = \frac{[p(s)]^2}{\rho} - \alpha\xi$. Therefore,

$$\xi(t) = e^{-\alpha t} \xi(0) + \int_0^t e^{-\alpha(t-s)} \frac{[p(s)]^2}{\rho} ds.$$

This means that, $\xi(t) \geq 0$ for all $t > 0$, given $\xi(0) \geq 0$. Therefore ξ can be seen as a friction coefficient, similarly to γ . We next show that under some conditions on f the dynamics of (6) is well-posed on infinite time horizons.

Lemma 1. *Assume that f is smooth and $f(x) \rightarrow +\infty$ as $\|x\| \rightarrow +\infty$. Then, for any initial condition $(x_0, p_0, \xi_0) \in \mathbb{R}^d \times \mathbb{R}^d \times \mathbb{R}_+$, the solution of (6) is well defined for all times $t \geq 0$, and there exists $R > 0$ such that*

$$\forall t \geq 0, \quad \|x(t)\| \leq R, \quad \|p(t)\| \leq R, \quad \|\xi(t)\| \leq R.$$

Proof. The Cauchy–Lipschitz theorem ensures the existence and uniqueness of a solution for a positive time. To show that the solution is global in time, we introduce the following Lyapunov function

$$\mathcal{G}(x, p, \xi) = f(x) - f(x^*) + \frac{1}{2} \|p\|^2 + \frac{\rho}{2} \|\xi\|^2.$$

The function $\mathcal{G}(t) = \mathcal{G}(x(t), p(t), \xi(t))$ satisfies

$$\begin{aligned} \dot{\mathcal{G}}(t) &= \nabla f(x(t)) \cdot \dot{x}(t) + p(t) \cdot \dot{p}(t) + \rho \xi(t) \cdot \dot{\xi}(t) \\ &= -\gamma \|p(t)\|^2 - (\xi(t) * p(t)) \cdot p(t) + \xi(t) \cdot [p(t)]^2 - \alpha \rho \|\xi(t)\|^2 \\ &= -\gamma \|p(t)\|^2 - \alpha \rho \|\xi(t)\|^2 \leq 0, \end{aligned}$$

where we used that $\xi(t) \geq 0$. This shows that $\mathcal{G}(t) \leq \mathcal{G}(0)$, from which the result easily follows since $f(x) - f(x^*) \geq 0$, $\forall x \in \mathbb{R}^d$. \square

The next result, whose derivation is straightforward, characterizes equilibria of the dynamics.

Proposition 1. *The equilibria of the system (6) correspond to*

$$(\dot{x}, \dot{p}, \dot{\xi}) = 0 \Rightarrow (p^*, -\nabla f(x^*), \xi^*) = 0,$$

i.e. they coincide with the physical equilibria.

H.2 Exponential convergence of the continuous iKFAD dynamics

Next, we show exponential convergence of the iKFAD dynamics (6) to the equilibria of Proposition 1.

Theorem 1. *Consider a function $f \in C^2$ and assume that there exist $a, b > 0$ such that*

$$\begin{aligned} a[f(x) - f(x^*)] + b\|x - x^*\|^2 \\ \leq (x - x^*) \cdot (\nabla f(x) - \nabla f(x^*)). \end{aligned} \quad (9)$$

Then, for any initial condition $(x_0, p_0, \xi_0) \in \mathbb{R}^d \times \mathbb{R}^d \times \mathbb{R}_+$, and considering $\gamma > 0$, there exist $\kappa > 0$ and $C \in \mathbb{R}_+$ such that the solution of (6) satisfies

$$f(x(t)) - f(x^*) + \|p(t)\| + \|\xi(t)\| \leq C e^{-\kappa t}.$$

Proof. Consider $\varepsilon > 0$ and introduce the following Lyapunov function (which is, up to the additional term $\|\xi\|^2$, a common choice for stochastic Langevin dynamics [18], also considered for dissipated Hamiltonian dynamics [19]):

$$\mathcal{W}_\varepsilon(x, p, \xi) = f(x) - f(x^*) + \frac{1}{2}\|p\|^2 + \frac{\rho}{2}\|\xi\|^2 + \varepsilon(x - x^*) \cdot p + \varepsilon\|x(t) - x^*\|^2. \quad (14)$$

We first derive a lower bound for $\mathcal{W}(t)$ which ensures positivity of the Lyapunov function.

$$\begin{aligned} \mathcal{W}(t) &= f(x) - f(x^*) + \frac{\rho}{2}\|\xi\|^2 + \frac{1}{4}\|p\|^2 + \frac{1}{4}\|p\|^2 + 2\varepsilon(x - x^*) \cdot \frac{p}{2} + \varepsilon^2\|x - x^*\|^2 - \varepsilon^2\|x - x^*\|^2 \\ &+ \frac{\varepsilon}{2}\|x - x^*\|^2 + \frac{\varepsilon}{2}\|x - x^*\|^2 \\ &= f(x) - f(x^*) + \frac{\rho}{2}\|\xi\|^2 + \frac{1}{4}\|p\|^2 + \left\| \frac{p}{2} + \varepsilon(x - x^*) \right\|^2 + \left(\frac{\varepsilon}{2} - \varepsilon^2 \right)\|x - x^*\|^2 + \frac{\varepsilon}{2}\|x - x^*\|^2. \end{aligned}$$

Assuming $\varepsilon \in [0, 1/2]$, we then have the following lower bound for the Lyapunov function (14)

$$\mathcal{W}_\varepsilon(x, p, \xi) \geq f(x) - f(x^*) + \frac{1}{4}\|p\|^2 + \frac{\rho}{2}\|\xi\|^2 + \frac{\varepsilon}{2}\|x - x^*\|^2, \quad (15)$$

We can similarly derive an upper bound for $\mathcal{W}_\varepsilon(x, p, \xi)$ as follows

$$\begin{aligned} \mathcal{W}(t) &= f(x) - f(x^*) + \frac{\rho}{2}\|\xi\|^2 + \frac{3}{4}\|p\|^2 - \frac{1}{4}\|p\|^2 + 2\varepsilon(x - x^*) \cdot \frac{p}{2} - \varepsilon^2\|x - x^*\|^2 \\ &+ \varepsilon^2\|x - x^*\|^2 + \frac{3\varepsilon}{2}\|x - x^*\|^2 - \frac{\varepsilon}{2}\|x - x^*\|^2 \\ &= f(x) - f(x^*) + \frac{\rho}{2}\|\xi\|^2 + \frac{3}{4}\|p\|^2 - \left(\left\| \frac{p}{4} - \varepsilon(x - x^*) \right\|^2 + \left[\frac{\varepsilon}{2} - \varepsilon^2 \right]\|x - x^*\|^2 \right) \\ &+ \frac{3\varepsilon}{2}\|x - x^*\|^2. \end{aligned}$$

As we have assumed $\varepsilon \in [0, 1/2]$, we then have the following upper bound

$$\mathcal{W}_\varepsilon(x, p, \xi) \leq f(x) - f(x^*) + \frac{3}{4}\|p\|^2 + \frac{\rho}{2}\|\xi\|^2 + \frac{3\varepsilon}{2}\|x - x^*\|^2. \quad (16)$$

We can then upper bound the time derivative of $\mathcal{W}_\varepsilon(t) = \mathcal{W}_\varepsilon(x(t), p(t), \xi(t))$ as follows

$$\begin{aligned} \dot{\mathcal{W}}_\varepsilon(t) &= \nabla f(x(t)) \cdot \dot{x}(t) + p(t) \cdot \dot{p}(t) + \rho \xi(t) \cdot \dot{\xi}(t) + \varepsilon p(t) \cdot \dot{x}(t) \\ &+ \varepsilon \dot{p}(t) \cdot (x(t) - x^*) + 2\varepsilon \dot{x}(t) \cdot (x(t) - x^*) \\ &= -(\gamma - \varepsilon)\|p(t)\|^2 - \alpha \rho \|\xi(t)\|^2 - \varepsilon(x(t) - x^*) \cdot \nabla f(x(t)) \\ &- \varepsilon(\gamma - 2)(x(t) - x^*) \cdot p(t) - \varepsilon(x(t) - x^*) \cdot (\xi \ast p) \\ &\leq -(\gamma - \varepsilon)\|p(t)\|^2 - \alpha \rho \|\xi(t)\|^2 - \varepsilon(x(t) - x^*) \cdot \nabla f(x(t)) \\ &+ \varepsilon |\gamma - 2| \left(\eta \|x(t) - x^*\|^2 + \frac{1}{4\eta} \|p(t)\|^2 \right) + \varepsilon \left(\Delta \|x(t) - x^*\|^2 + \frac{R^2}{4\Delta} \|p(t)\|^2 \right), \end{aligned}$$

where we used weighted Young's inequalities as well as Lemma 1. Specifically, we used that $\|\xi\| \leq R$ so that $\xi_i^2 \leq R^2$ in particular. We can therefore bound $\|\xi * p\|^2$ as $\|\xi * p\|^2 = \sum (\xi_i p_i)^2 \leq R^2 \|p\|^2$. Using assumption (9), we have

$$\begin{aligned} \dot{\mathcal{W}}_\varepsilon(t) &\leq -\left[\gamma - \varepsilon \left(1 - \frac{R^2}{4\Delta} - \frac{|\gamma-2|}{4\eta} \right) \right] \|p(t)\|^2 - \alpha\rho \|\xi(t)\|^2 - a\varepsilon(f(x) - f(x^*)) \\ &\quad - \varepsilon \left(b - |\gamma-2|\eta - \Delta \right) \|x(t) - x^*\|^2. \end{aligned}$$

We set $\eta = \frac{b}{4|\gamma-2|}$ and $\Delta = b/4$, upon which, we obtain

$$\begin{aligned} \dot{\mathcal{W}}_\varepsilon(t) &\leq -\left[\gamma - \varepsilon \left(1 - \frac{R^2 + (\gamma-2)^2}{b} \right) \right] \|p(t)\|^2 - \alpha\rho \|\xi(t)\|^2 - a\varepsilon(f(x) - f(x^*)) \\ &\quad - \frac{\varepsilon b}{2} \|x(t) - x^*\|^2. \end{aligned}$$

Using (16), we obtain the following upper bound for the time derivative of the Lyapunov function (14)

$$\dot{\mathcal{W}}_\varepsilon(t) \leq -\min \left\{ \frac{4}{3} \left[\gamma - \varepsilon \left(1 - \frac{R^2 - (\gamma-2)^2}{b} \right) \right], 2\alpha, a\varepsilon, \frac{b}{3} \right\} \mathcal{W}_\varepsilon(t).$$

Considering a sufficiently small ε , the above upper bound gives us the desired exponential convergence result through the use of Grönwall's inequality. \square

H.3 Discrete Convergence Analysis

Consider the following splitting of the continuous dynamics (6)

$$\begin{pmatrix} \dot{x} \\ \dot{p} \\ \dot{\xi} \end{pmatrix} = \underbrace{\begin{pmatrix} p \\ 0 \\ 0 \end{pmatrix}}_{\mathbf{A}} + \underbrace{\begin{pmatrix} 0 \\ -\nabla f(x) \\ 0 \end{pmatrix}}_{\mathbf{B}} + \underbrace{\begin{pmatrix} 0 \\ -\xi * p \\ \frac{\|p\|^2}{\rho} \end{pmatrix}}_{\mathbf{C}} + \underbrace{\begin{pmatrix} 0 \\ -\gamma p \\ -\alpha \xi \end{pmatrix}}_{\mathbf{D}}, \quad (17)$$

and the integration scheme $C'DBA$. For step C' , similarly to the analysis performed in [9], we observe that $p_i^2 + \rho \xi_i^2$ is an invariant quantity. Using this, and defining $\Xi = \text{diag}(\xi)$, the integration scheme $C'DBA$ can be written as follows

$$\text{Step } C' \quad \tilde{p}_{n+1/2} = e^{-\Xi_n \delta t} p_n \quad (18)$$

$$\tilde{\xi}_{n+1} = \sqrt{[\xi_n]^2 + \frac{(I - e^{-2\Xi_n \Delta t})}{\rho} [p_n]^2} \quad (19)$$

$$\text{Step } D \quad \tilde{p}_{n+1} = e^{-\gamma \delta t} \tilde{p}_{n+1/2} \quad (20)$$

$$\xi_{n+1} = e^{-\alpha \delta t} \tilde{\xi}_{n+1} \quad (21)$$

$$\text{Step } B \quad p_{n+1} = \tilde{p}_{n+1} - \delta t \nabla f(x_n) \quad (22)$$

$$\text{Step } A \quad x_{n+1} = x_n + \delta t p_{n+1} \quad (23)$$

where for the C' step, we first fix ξ and analytically solve $\dot{p}_i = -\xi * p_i \Rightarrow p_{n+1,i} = p_{n,i} e^{-\xi_{n,i} t}$, which, in vector form corresponds to Equation (18). We then update ξ by observing that for the C' step $\frac{d}{dt} (p_i^2 + \rho \xi_i^2) = 2p_i \dot{p}_i + 2\rho \xi_i \dot{\xi}_i = 2p_i (-\xi_i * p_i) + 2\rho \xi_i \frac{p_i^2}{\rho} = 0$. We therefore have $p_{n+1,i}^2 + \rho \xi_{n+1,i}^2 = p_{n,i}^2 + \rho \xi_{n,i}^2 \Rightarrow \xi_{n+1,i}^2 = \xi_{n,i}^2 + \frac{p_{n,i}^2 - p_{n+1,i}^2}{\rho}$. This, written in vector form, yields the update rule for ξ in Equation (19).

Upon defining $\beta_{n,\delta t} = e^{-(\gamma I + \Xi_n) \delta t}$, we can rewrite equations (18)-(23) as

$$p_{n+1} = \beta_{n,\delta t} p_n - \delta t \nabla f(x_n) \quad (24a)$$

$$x_{n+1} = x_n + \delta t \beta_{n,\delta t} p_n - \delta t^2 \nabla f(x_n) \quad (24b)$$

$$\xi_{n+1} = e^{-\alpha \delta t} \sqrt{[\xi_n]^2 + \frac{(I - e^{-2\Xi_n \delta t}) [p_n]^2}{\rho}}. \quad (24c)$$

Equations (24) are a restatement of the system of equations (10). We now show that every equilibrium point of the discrete dynamics is also an equilibrium point of the continuous dynamics, thus the discretization does not introduce any ‘‘artificial’’ equilibrium points. Conversely, we also show that every equilibrium of the continuous dynamics is also an equilibrium of the discrete dynamics.

Proposition 2. *A state $s = (x, p, \xi)$ is an equilibrium point of the discrete iKFAD dynamics given by equations (10a)-(10c) if and only if it is an equilibrium of the continuous iKFAD dynamics (6).*

Proof. Let s^* be an equilibrium of the continuous dynamics as described in Proposition 1 and let $s_n = (x_n, p_n, \xi_n)$ be an equilibrium point of the discrete dynamics (10a)-(10c). This implies that if we take a step of the discrete dynamics starting from s_n , we will remain at equilibrium, that is $s_{n+1} = s_n$. Using equation (23) and setting $x_{n+1} = x_n$ gives us $p_{n+1} = 0$ which implies $p_n = p_{n+1} = 0$. Substituting $p_n = 0$ into Equation (24c) and using $\xi_{n+1} = \xi_n$, yields $\xi_n = e^{-\alpha\delta t}\xi_n$, so that $\xi_n = 0$ as $\alpha\delta t > 0$. Finally, for $p_{n+1} = p_n = 0$, equation (10a) yields $\nabla f(x_n) = 0$.

We next show that any equilibrium point of the continuous dynamics is also an equilibrium of the discrete dynamics. Consider an equilibrium $s^* = (x^*, p^*, \xi^*) = (x^*, 0, 0)$ such that $\nabla f(x^*) = 0$. Let $s_n = s^*$ and let us take a step following the discrete dynamics as given by equations (10a)-(10c). It is straightforward to see that $z_n = (x^*, 0, 0)$ leads to $s_{n+1} = s_n = s^*$. \square

Next, we establish convergence to the minimizer for the discrete-time dynamics in Equations (24).

Theorem 2. *Consider a function $f \in C^2$ satisfying $0 < m \leq \nabla^2 f(x) \leq M < +\infty$. Assume that $\gamma > 0$ and consider $L > 0$. Then, for any initial condition $(x_0, p_0, \xi_0) \in \mathbb{R}^d \times \mathbb{R}^d \times \mathbb{R}^d$ such that*

$$\|x_0\| + \|p_0\| + \|\xi_0\| \leq L,$$

there exist $\delta t^ > 0$, $\kappa > 0$ and $C > 0$ (depending on L) such that $\forall \delta t \in (0, \delta t^*)$, $\forall n \geq 0$,*

$$f(x_n) - f(x^*) + \|p_n\|^2 + \|\xi_n\|^2 \leq C e^{-\kappa n \delta t}.$$

Proof. This proof follows the same steps as the convergence analysis of the discretized FAD dynamics presented in [9], the only difference being the fact that ξ in the iKFAD dynamics is a vector, rather than a scalar (as was the case for FAD), and that the matrix $A(x)$ involved in the FAD dynamics is now taken to be the identity $A(x) = I$. Without loss of generality (upon translating and adding a constant to $f(x)$) we can assume that $f(x^*) = 0$ and $x^* = 0$. We consider the Lyapunov function

$$\mathcal{W}(x, p, \xi) = f(x) + \frac{1}{2}\|p\|^2 + A_{\delta t}\rho\|\xi\|^2 + B_{\delta t}\|x\|^2 + C_{\delta t}x \cdot p, \quad (25)$$

which is the Lyapunov function of Equation (14), with coefficients $A_{\delta t}, B_{\delta t}, C_{\delta t}$ to be determined. We can rewrite Equation (25) as

$$\mathcal{W}(x, p, \xi) = f(x) + A_{\delta t}\rho\|\xi\|^2 + [x \quad p] \begin{bmatrix} B_{\delta t} & C_{\delta t}/2 \\ C_{\delta t}/2 & 1/2 \end{bmatrix} \begin{bmatrix} x \\ p \end{bmatrix}.$$

To ensure positivity of $\mathcal{W}(x, p, \xi)$, we need $\det \begin{pmatrix} B_{\delta t} & C_{\delta t}/2 \\ C_{\delta t}/2 & 1/2 \end{pmatrix} > 0 \Rightarrow B_{\delta t} > C_{\delta t}^2/2$ and also want $A_{\delta t} > 0$. We start by expressing each of the terms in the Lyapunov function at step $n+1$ as a function of corresponding terms at step n and deriving upper bounds where possible. Using the fact that $\nabla^2 f(x) \leq M$ we can derive the following upper bound for $f(x_{n+1})$:

$$\begin{aligned} f(x_{n+1}) &\leq f(x_n) + \nabla f(x_n) \cdot (x_{n+1} - x_n) + \frac{M}{2}\|x_{n+1} - x_n\|^2 \\ &\leq f(x_n) + \delta t\beta_{n,\delta t}p_n \cdot \nabla f(x_n) + C\delta t^2(\|p_n\|^2 + \|\nabla f(x_n)\|^2). \end{aligned}$$

Next,

$$\begin{aligned} \|x_{n+1}\|^2 &= \|x_n + \delta t\beta_{n,\delta t}p_n - \delta t^2\nabla f(x_n)\|^2 \\ &\leq \|x_n\|^2 + 2\delta t\beta_{n,\delta t}x_n \cdot p_n - 2\delta t^2x_n \cdot \nabla f(x_n) + C\delta t^2(\|p_n\|^2 + \|\nabla f(x_n)\|^2). \end{aligned}$$

We also have

$$\begin{aligned} \|p_{n+1}\|^2 &= \|\beta_{n,\delta t}p_n - \delta t\nabla f(x_n)\|^2 \\ &= p_n \cdot \beta_{n,2\delta t}p_n - 2\delta t\beta_{n,\delta t}p_n \cdot \nabla f(x_n) + \delta t^2\|\nabla f(x_n)\|^2. \end{aligned}$$

Moreover,

$$\begin{aligned} x_{n+1} \cdot p_{n+1} &= \beta_{n,\delta t} p_n \cdot x_n - \delta t x_n \cdot \nabla f(x_n) + \delta t \|\beta_{n,\delta t} p_n\|^2 \\ &\quad - 2\delta t^2 \beta_{n,\delta t} p_n \cdot \nabla f(x_n) + \delta t^3 \|\nabla f(x_n)\|^2 \\ &\leq x_n \cdot p_n - \delta t x_n \cdot \nabla f(x_n) - (I - \beta_{n,\delta t}) x_n \cdot p_n \\ &\quad + \delta t p_n \cdot \beta_{n,2\delta t} p_n + C\delta t^2 (\|p_n\|^2 + \|\nabla f(x_n)\|^2). \end{aligned}$$

Finally, we have

$$\rho \|\xi_{n+1}\|^2 = e^{-2\alpha\delta t} [p_n^T (I - e^{-2\Xi_n \delta t}) p_n + \rho \|\xi_n\|^2].$$

Given the above, we have the following upper bound for the Lyapunov function at step $n+1$:

$$\begin{aligned} \mathcal{W}(x_{n+1}, p_{n+1}, \xi_{n+1}) &\leq \mathcal{W}(x_n, p_n, \xi_n) - A_{\delta t} (1 - e^{-2\alpha\delta t}) \rho \|\xi_n\|^2 \\ &\quad + [(2B_{\delta t} \delta t \beta_{n,\delta t} - C_{\delta t} (I - \beta_{n,\delta t})) p_n] \cdot x_n - (C_{\delta t} + 2B_{\delta t} \delta t) \delta t x_n \cdot \nabla f(x_n) \\ &\quad - \left[\frac{1}{2} - A_{\delta t} e^{-2\alpha\delta t} - C_{\delta t} \delta t e^{-2\gamma\delta t} \right] \|p_n\|^2 + \left[\frac{e^{-2\gamma\delta t}}{2} - A_{\delta t} e^{-2\alpha\delta t} \right] p_n^T e^{-2\Xi_n \Delta t} p_n \\ &\quad + C\delta t^2 (\|p_n\|^2 + \|\nabla f(x_n)\|^2). \end{aligned}$$

We choose $A_{\delta t} = \frac{1}{2} e^{2(\alpha-\gamma)\delta t}$, which eliminates the term proportional to $p_n^T e^{-2\Xi_n \delta t} p_n$. This gives us

$$\begin{aligned} \mathcal{W}(x_{n+1}, p_{n+1}, \xi_{n+1}) &\leq \mathcal{W}(x_n, p_n, \xi_n) - \frac{e^{2(\alpha-\gamma)\delta t}}{2} (1 - e^{-2\alpha\delta t}) \rho \|\xi_n\|^2 \\ &\quad + [(2B_{\delta t} \delta t \beta_{n,\delta t} - C_{\delta t} (I - \beta_{n,\delta t})) p_n] \cdot x_n - (C_{\delta t} + 2B_{\delta t} \delta t) \delta t x_n \cdot \nabla f(x_n) \\ &\quad - \left[\frac{1 - e^{-2\gamma\delta t}}{2} - C_{\delta t} \delta t e^{-2\gamma\delta t} \right] \|p_n\|^2 + C\delta t^2 (\|p_n\|^2 + \|\nabla f(x_n)\|^2). \end{aligned}$$

Setting $B_{\delta t} = C_{\delta t} = \varepsilon > 0$, choosing $\varepsilon, \delta t$ to be sufficiently small and using that $x \cdot \nabla f(x) \geq 0$, we obtain

$$\begin{aligned} \mathcal{W}(x_{n+1}, p_{n+1}, \xi_{n+1}) &\leq \mathcal{W}(x_n, p_n, \xi_n) - \alpha \rho \delta t \|\xi_n\|^2 - \gamma \delta t \|p_n\|^2 - \varepsilon \delta t x_n \cdot \nabla f(x_n) \\ &\quad + \varepsilon ([2\delta t \beta_{n,\delta t} - (I - \beta_{n,\delta t})] p_n) \cdot x_n + C\delta t^2 (\|p_n\|^2 + \|\nabla f(x_n)\|^2). \end{aligned}$$

The assumption $0 < m < \nabla^2 f(x) \leq M$ together with the equalities $f(0) = 0$ and $\nabla f(0) = 0$ implies through Taylor expansions with integral remainder that $f(x) \geq m\|x\|^2/2$ and $\|\nabla f(x)\| \leq M\|x\|$. In view of these two inequalities, there exists $K \in \mathbb{R}_+$ such that, uniformly in $\varepsilon \in (0, 1/2]$,

$$\|p\|^2 + \|\nabla f(x)\|^2 \leq K \mathcal{W}(x, p, \xi).$$

Since $B_{\delta t} > C_{\delta t}^2/2$ and $A_{\delta t} > 0$, we have $A_{\delta t} \rho \|\xi_n\|^2 \leq \mathcal{W}(x_n, p_n, \xi_n)$ so that $\|\xi_n\| \leq \sqrt{\mathcal{W}(x_n, p_n, \xi_n)/(A_{\delta t} \rho)}$. Let us fix $R > 0$ and define $\mathcal{W}_R = A_{\delta t} \rho R^2$. Then, whenever $\mathcal{W}(x_n, p_n, \xi_n) \leq \mathcal{W}_R$ holds, we can deduce $\|\xi_n\| \leq R$ and therefore

$$\|I - \beta_{n,\delta t}\| = \|I - e^{-(\gamma I + \Xi_n)\delta t}\| \leq 1 - e^{-(\gamma+R)\delta t}.$$

We now conclude the proof by induction. Assume $\mathcal{W}(x_n, p_n, \xi_n) \leq \mathcal{W}_R$. Using the above bound on $\|I - \beta_{n,\delta t}\|$, we obtain

$$\begin{aligned} \mathcal{W}(x_{n+1}, p_{n+1}, \xi_{n+1}) &\leq (1 + CK\delta t^2) \mathcal{W}(x_n, p_n, \xi_n) - \alpha \rho \delta t \|\xi_n\|^2 - \gamma \delta t \|p_n\|^2 - \varepsilon \delta t x_n \cdot \nabla f(x_n) \\ &\quad + \varepsilon (2\delta t + 1 - e^{-(\gamma+R)\delta t}) \|p_n\| \|x_n\| \\ &\leq (1 + CK\delta t^2) \mathcal{W}(x_n, p_n, \xi_n) - \alpha \rho \delta t \|\xi_n\|^2 \\ &\quad - \varepsilon \delta t \left(x_n \cdot \nabla f(x_n) - \eta \frac{|2\delta t + 1 - e^{-(\gamma+R)\delta t}|}{\delta t} \|x_n\|^2 \right) \\ &\quad - \delta t \left(\gamma - \frac{\varepsilon}{4\eta} \frac{|2\delta t + 1 - e^{-(\gamma+R)\delta t}|}{\delta t} \right) \|p_n\|^2. \end{aligned}$$

Note that we can then use the strong convexity inequality to bound $-x_n \cdot \nabla f(x_n) \leq -f(x_n) - \frac{m}{2} \|x\|^2 \leq m\|x\|^2$, upon which, the third term in the above inequality can be written as

$$-\varepsilon \delta t \left(x_n \cdot \nabla f(x_n) - \eta \frac{|2\delta t + 1 - e^{-(\gamma+R)\delta t}|}{\delta t} \|x_n\|^2 \right) = -\varepsilon \delta t \left(m - \eta \frac{|2\delta t + 1 - e^{-(\gamma+R)\delta t}|}{\delta t} \right) \|x_n\|^2.$$

The constant η then needs to be chosen sufficiently small, so that $m - \eta \frac{|2\delta t + 1 - e^{-(\gamma+R)\delta t}|}{\delta t} > 0$. Similarly, we must choose a sufficiently small ε in order to ensure positivity of the term $\gamma - \frac{\varepsilon}{4\eta} \frac{|2\delta t + 1 - e^{-(\gamma+R)\delta t}|}{\delta t} > 0$. We can then group terms of $O(\delta t)$, upon which we get a term of the form $O(\delta t)(\|x_n\|^2 + \|p_n\|^2 + \|\xi_n\|^2)$. From the definition of the Lyapunov function and upon completing the squares we can obtain an inequality of the form

$$\mathcal{W}(x_n, p_n, \xi_n) \leq C(\|x_n\|^2 + \|p_n\|^2 + \|\xi_n\|^2) \Rightarrow -O(\delta t)(\|x_n\|^2 + \|p_n\|^2 + \|\xi_n\|^2) \leq -\mathcal{W}(x_n, p_n, \xi_n).$$

The above implies that there exists $\kappa > 0$, such that

$$\mathcal{W}(x_{n+1}, p_{n+1}, \xi_{n+1}) \leq (1 - \kappa\delta t + CK\delta t^2)\mathcal{W}(x_n, p_n, \xi_n).$$

For a sufficiently small step-size δt , so that $0 < (1 - \kappa\delta t + CK\delta t^2) < 1$, the right hand side of the above inequality can be upper bounded by \mathcal{W}_R , which proves that the induction hypothesis also holds for $n + 1$. This allows us to conclude the claimed exponential convergence result. \square

I CD convergence analysis

This section establishes the convergence properties of the proposed CD optimizer. We first prove that the continuous-time CD dynamics converge at an exponential rate to the global minimum. We then show that this exponential (geometric) rate is preserved in discrete time, provided the step size δt is sufficiently small.

I.1 Dynamical properties of CD

In this section we study the dynamical properties of the system (7). We propose a Lyapunov function to prove exponential convergence of the dynamics under the assumption that f is strongly convex.

A first result is that the dynamics is well posed on infinite time horizons under some conditions on f .

Lemma 2. *Assume that f is a smooth function, such that $f(x) \rightarrow \infty$ as $\|x\| \rightarrow +\infty$. Then, for any initial condition $(x_0, p_0) \in \mathbb{R}^d \times \mathbb{R}^d$, the solution of (7) is well defined for all times $t \geq 0$ and there exists $R \in \mathbb{R}_+$ such that $\|x(t)\| \leq R$ and $\|p(t)\| \leq R$, for any $t \geq 0$.*

Proof. Existence and uniqueness of a local in time solution of (7) follow from the Cauchy-Lipschitz theorem. To prove that the solution is global in time we define the following Lyapunov function

$$\mathcal{G}(x, p, \xi) = f(x) - f(x^*) + \frac{1}{2}\|p\|^2.$$

A simple computation shows that the function $\mathcal{G}(t) = \mathcal{G}(x(t), p(t), \xi(t))$ satisfies

$$\begin{aligned} \dot{\mathcal{G}}(t) &= \nabla f(x(t)) \cdot \dot{x}(t) + p(t) \cdot \dot{p}(t) \\ &= -\gamma\|p(t)\|^2 - cp(t) \cdot [p(t)]^3 \leq 0, \end{aligned}$$

since $\gamma, c \geq 0$. This means that $\mathcal{G}(t) \leq \mathcal{G}(0)$, from which the result easily follows since $f - f(x^*)$ and $\|p\|^2$ are non-negative. \square

The next proposition, whose proof is immediate, characterizes the equilibria of the dynamics.

Proposition 3. *The equilibria of the system (7) coincide with the physical equilibria, i.e.*

$$(\dot{x}, \dot{p}) = 0 \Leftrightarrow (p^*, \nabla f(x^*)) = 0.$$

I.2 Exponential convergence of the continuous CD dynamics

Theorem 3. *Consider a function $f \in C^2$. Assume that $\gamma, c > 0$ and that there exist $a, b > 0$ such that*

$$\begin{aligned} a[f(x) - f(x^*)] + b\|x - x^*\|^2 \\ \leq (x - x^*) \cdot (\nabla f(x) - \nabla f(x^*)). \end{aligned} \tag{11}$$

Then, for any initial condition $(x_0, p_0, \xi_0) \in \mathbb{R}^d \times \mathbb{R}^d \times \mathbb{R}_+$, there exist $\kappa > 0$ and $C \in \mathbb{R}_+$ such that the solution of (7) satisfies

$$f(x(t)) - f(x^*) + \|p(t)\| \leq Ce^{-\kappa t}.$$

Proof. Similarly to the steps followed for the proof of Theorem 1, we consider the Lyapunov function

$$\mathcal{W}_\varepsilon(x, p) = f(x) - f(x^*) + \frac{1}{2}\|p\|^2 + \varepsilon(x - x^*) \cdot p + \varepsilon\|x - x^*\|^2. \quad (26)$$

for which the following upper bound can be derived (for $\varepsilon \in [0, 1/2]$)

$$\mathcal{W}_\varepsilon(x, p) \leq f(x) - f(x^*) + \frac{3}{4}\|p\|^2 + \frac{3\varepsilon}{2}\|x - x^*\|^2. \quad (27)$$

Differentiating $\dot{\mathcal{W}}_\varepsilon(t) = \mathcal{W}_\varepsilon(x(t), p(t))$ with respect to time, we obtain

$$\begin{aligned} \dot{\mathcal{W}}_\varepsilon(t) &= \nabla f(x(t)) \cdot \dot{x}(t) + p(t) \cdot \dot{p}(t) + \varepsilon \dot{x}(t) \cdot p(t) \\ &\quad + \varepsilon(x(t) - x^*) \cdot \dot{p}(t) + 2\varepsilon(x(t) - x^*) \cdot \dot{x}(t) \\ &= -(\gamma - \varepsilon)\|p(t)\|^2 - \varepsilon(x(t) - x^*) \cdot \nabla f(x(t)) \\ &\quad + \varepsilon(2 - \gamma)(x(t) - x^*) \cdot p(t) - c\varepsilon(x(t) - x^*) \cdot [p(t)]^3 - cp(t) \cdot [p(t)]^3 \\ &\leq -(\gamma - \varepsilon)\|p(t)\|^2 - \varepsilon(x(t) - x^*) \cdot \nabla f(x(t)) \\ &\quad + \varepsilon|\gamma - 2|\left(\Delta\|x(t) - x^*\|^2 + \frac{1}{4\Delta}\|p(t)\|^2\right) + c\varepsilon\left(\eta\|x(t) - x^*\|^2 + \frac{R^4}{4\eta}\|p(t)\|^2\right), \end{aligned}$$

where we used a Cauchy–Schwarz inequality to bound the last two terms, as well as Lemma 2 to bound the term $\|[p]^3\|^2$ as follows: $\|[p]^3\|^2 = \sum(p_i^3)^2 = \sum(p_i^2)^3 \leq (\sum p_i^2)^3 = (\|p\|^2)^3 \leq \|p\|^2 R^4$. We have also used the fact that $p \cdot p^3 \geq 0$.

In view of Condition (11), we can write

$$\dot{\mathcal{W}}_\varepsilon(t) \leq -a\varepsilon(f(x(t)) - f(x^*)) - \left(\gamma - \varepsilon\left(1 + \frac{(\gamma - 2)^2}{b} + c^2\frac{R^4}{b}\right)\right)\|p(t)\|^2 - \frac{b\varepsilon}{2}\|x(t) - x^*\|^2,$$

where we set $\Delta = \frac{b}{4|\gamma - 2|}$ and $\eta = \frac{b}{4c}$. This bound for $\dot{\mathcal{W}}_\varepsilon(t)$, combined with the upper bound in equation (27) yields

$$\dot{\mathcal{W}}_\varepsilon(t) \leq -\min\left\{a\varepsilon, \frac{b}{3}, \frac{4}{3}\left(\gamma - \varepsilon\left(1 + \frac{(\gamma - 2)^2}{b} + c^2\frac{R^4}{b}\right)\right)\right\}\mathcal{W}_\varepsilon$$

For a sufficiently small ε we can use Gronwall's inequality to conclude to an exponential convergence of the dynamics (7). \square

I.3 Discrete Convergence Analysis

We consider the following Euler discretization of the continuous CD equations (7), which is simpler to analyze than a splitting scheme:

$$\begin{aligned} p_{n+1} &= (1 - \gamma\delta t)p_n - c\delta t[p_n]^3 - \delta t\nabla f(x_n), \\ x_{n+1} &= x_n + \delta t p_n, \end{aligned}$$

where we assume $\gamma\delta t$ is sufficiently small. The above discretization scheme coincides with Equations (12a)–(12b) and is restated here for completeness. We next consider a perturbation of the Lyapunov function (26), namely

$$\mathcal{W}_{\delta t}(x_n, p_n) = f(x_n) + A_{\delta t}\frac{\|p_n\|^2}{2} + B_{\delta t}\|x_n\|^2 + C_{\delta t}x_n \cdot p_n, \quad (28)$$

where $A_{\delta t} > 0$ and $B_{\delta t} > \frac{C_{\delta t}^2}{2A_{\delta t}}$.

Theorem 4. Consider $f \in C^2$ and assume that there exist $m, M \in \mathbb{R}_+$ such that $m \leq \nabla^2 f(x) \leq M \forall x \in \mathbb{R}^N$. Fix $L > 0$, then, for any initial condition (x_0, p_0) such that $\|x_0\| + \|p_0\| \leq L$, there exists $\delta t^* > 0$, $r > 0$ and $C > 0$ for which

$$\begin{aligned} \forall n \geq 0 \text{ and } \forall \delta t \in (0, \delta t^*), \\ f(x_n) - f(x^*) + \|p_n\|^2 \leq Ce^{-\kappa n \delta t}. \end{aligned}$$

Proof. We begin the proof by upper bounding/expanding each of the terms in the Lyapunov function at step $n + 1$. Since $0 \leq \nabla^2 f(x) \leq M$ we have

$$f(x_{n+1}) \leq f(x_n) + \delta t \nabla f(x_n) \cdot p_n + \frac{\delta t^2 M}{2} \|p_n\|^2.$$

We assume that $\gamma \delta t \leq 1$. We can bound terms of the form $\|p\|^3$ similarly to the continuous case, provided there exists $R > 0$ such that $\|p\| < R$. Such a bound on $\|p\|$ can be derived by induction. Since $B_{\delta t} > C_{\delta t}^2 / (2A_{\delta t})$ and $A_{\delta t} > 0$, the quadratic form in (x, p) is positive definite and together with $f(x) \geq \frac{m}{2} \|x\|^2$, this implies that there exists $c_0 > 0$ such that $c_0 \|p_n\|^2 \leq c_0 (\|x_n\|^2 + \|p_n\|^2) \leq \mathcal{W}(x_n, p_n)$. Hence, $\|p_n\| \leq \sqrt{\mathcal{W}(x_n, p_n) / c_0}$. Fix $R > 0$ and set $\mathcal{W}_R = c_0 R^2$. Then, whenever $\mathcal{W}(x_n, p_n) \leq \mathcal{W}_R$ holds, we can deduce $\|p_n\| \leq R$. We choose $R = R(L)$ so that $\mathcal{W}(x_0, p_0) \leq \mathcal{W}_R$ and proceed by induction assuming $\mathcal{W}(x_n, p_n) \leq \mathcal{W}_R$.

$$\begin{aligned} \|p_{n+1}\|^2 &= \|(1 - \gamma \delta t)p_n - c \delta t [p_n]^3 - \delta t \nabla f(x_n)\|^2 \\ &= \|(1 - \gamma \delta t)p_n - c \delta t [p_n]^3\|^2 - 2 \delta t \left[(1 - \gamma \delta t)p_n - c \delta t [p_n]^3 \right] \cdot \nabla f(x_n) + \|\nabla f(x_n)\|^2 \\ &= \|(1 - \gamma \delta t)p_n\|^2 - 2c(1 - \gamma \delta t) \delta t p_n \cdot [p_n]^3 + \|c \delta t [p_n]^3\|^2 \\ &\quad - 2 \left[(1 - \gamma \delta t)p_n - c \delta t [p_n]^3 \right] \delta t \nabla f(x_n) + \|\delta t \nabla f(x_n)\|^2 \\ &\leq (1 - \gamma \delta t)^2 \|p_n\|^2 + c^2 \delta t^2 R^4 \|p_n\|^2 \\ &\quad - 2 \delta t (1 - \gamma \delta t) p_n \cdot \nabla f(x_n) + 2c \delta t^2 [p_n]^3 \cdot \nabla f(x_n) + \delta t^2 \|\nabla f(x_n)\|^2 \\ &\leq \|p_n\|^2 - 2\gamma \delta t \|p_n\|^2 + \gamma^2 \delta t^2 \|p_n\|^2 + c^2 \delta t^2 R^4 \|p_n\|^2 \\ &\quad - 2 \delta t (1 - \gamma \delta t) p_n \cdot \nabla f(x_n) + 2c \delta t^2 \left(\frac{1}{4\theta} \|p_n\|^3 \|^2 + \theta \|\nabla f(x_n)\|^2 \right) + \delta t^2 \|\nabla f(x_n)\|^2 \\ &\leq \|p_n\|^2 - 2\gamma \delta t \|p_n\|^2 + \gamma^2 \delta t^2 \|p_n\|^2 + c^2 \delta t^2 R^4 \|p_n\|^2 \\ &\quad - 2 \delta t (1 - \gamma \delta t) p_n \cdot \nabla f(x_n) + 2c \delta t^2 \left(\frac{R^4}{4\theta} \|p_n\|^2 + \theta \|\nabla f(x_n)\|^2 \right) + \delta t^2 \|\nabla f(x_n)\|^2 \\ &= \|p_n\|^2 - 2\gamma \delta t \|p_n\|^2 + \gamma^2 \delta t^2 \|p_n\|^2 + c^2 \delta t^2 R^4 \|p_n\|^2 \\ &\quad - 2 \delta t p_n \cdot \nabla f(x_n) + 2\gamma \delta t^2 p_n \cdot \nabla f(x_n) + \frac{cR^4}{2\theta} \delta t^2 \|p_n\|^2 + 2c \delta t^2 \theta \|\nabla f(x_n)\|^2 + \delta t^2 \|\nabla f(x_n)\|^2 \\ &\leq \|p_n\|^2 - 2\gamma \delta t \|p_n\|^2 + \gamma^2 \delta t^2 \|p_n\|^2 + c^2 R^4 \delta t^2 \|p_n\|^2 - 2 \delta t p_n \cdot \nabla f(x_n) \\ &\quad + 2\gamma \delta t^2 \left(\frac{1}{4\xi} \|p_n\|^2 + \xi \|\nabla f(x_n)\|^2 \right) + \frac{cR^4}{2\theta} \delta t^2 \|p_n\|^2 + 2c \theta \delta t^2 \|\nabla f(x_n)\|^2 + \delta t^2 \|\nabla f(x_n)\|^2. \end{aligned}$$

Therefore

$$\|p_{n+1}\|^2 \leq \|p_n\|^2 - 2\gamma \delta t \|p_n\|^2 - 2 \delta t p_n \cdot \nabla f(x_n) + Q \delta t^2 \left(\|p_n\|^2 + \|\nabla f(x_n)\|^2 \right).$$

We also have

$$\|x_{n+1}\|^2 = \|x_n\|^2 + 2\delta t x_n \cdot p_n + \delta t^2 \|p_n\|^2.$$

Finally,

$$\begin{aligned} x_{n+1} \cdot p_{n+1} &= (x_n + \delta t p_n) \cdot ((1 - \gamma \delta t)p_n - c \delta t [p_n]^3 - \delta t \nabla f(x_n)) \\ &= (1 - \gamma \delta t)x_n \cdot p_n - c \delta t x_n \cdot [p_n]^3 - \delta t x_n \cdot \nabla f(x_n) \\ &\quad + (1 - \gamma \delta t)\delta t p_n \cdot p_n - c \delta t^2 p_n \cdot [p_n]^3 - \delta t^2 p_n \cdot \nabla f(x_n) \\ &\leq x_n \cdot p_n - \gamma \delta t x_n \cdot p_n + c \delta t |x_n \cdot [p_n]^3| - \delta t x_n \cdot \nabla f(x_n) \\ &\quad + \delta t \|p_n\|^2 - \gamma \delta t^2 \|p_n\|^2 + \delta t^2 \left(\frac{1}{4\kappa} \|p_n\|^2 + \kappa \|\nabla f(x_n)\|^2 \right) \\ &\leq x_n \cdot p_n - \gamma \delta t x_n \cdot p_n + c \delta t |x_n \cdot [p_n]^3| - \delta t x_n \cdot \nabla f(x_n) \\ &\quad + \delta t \|p_n\|^2 + \delta t^2 \left(\frac{1}{4\kappa} \|p_n\|^2 + \kappa \|\nabla f(x_n)\|^2 \right). \end{aligned}$$

We thus have

$$\begin{aligned}
\mathcal{W}(x_{n+1}, p_{n+1}) &\leq f(x_n) + \delta t \nabla f(x_n) \cdot p_n \\
&\quad + A_{\delta t} \frac{\|p_n\|^2}{2} - A_{\delta t} \gamma \delta t \|p_n\|^2 - A_{\delta t} \delta t \nabla f(x_n) \cdot p_n \\
&\quad + B_{\delta t} \|x_n\|^2 + 2B_{\delta t} \delta t \|x_n\| \|p_n\| \\
&\quad + C_{\delta t} x_n \cdot p_n + C_{\delta t} (\gamma + cR^2) \delta t \|x_n\| \|p_n\| - C_{\delta t} \delta t x_n \cdot \nabla f(x_n) + C_{\delta t} \delta t \|p_n\|^2 \\
&\quad + Q \delta t^2 (\|p_n\|^2 + \|\nabla f(x_n)\|^2) \\
&= \mathcal{W}(x_n, p_n) + (1 - A_{\delta t}) \delta t \nabla f(x_n) \cdot p_n \\
&\quad - A_{\delta t} \gamma \delta t \|p_n\|^2 + 2B_{\delta t} \delta t \|x_n\| \|p_n\| \\
&\quad + C_{\delta t} (\gamma + cR^2) \delta t \|x_n\| \|p_n\| - C_{\delta t} \delta t x_n \cdot \nabla f(x_n) + C_{\delta t} \delta t \|p_n\|^2 \\
&\quad + Q \delta t^2 (\|p_n\|^2 + \|\nabla f(x_n)\|^2) \\
&\leq \mathcal{W}(x_n, p_n) - C_{\delta t} \delta t x_n \cdot \nabla f(x_n) + (1 - A_{\delta t}) \delta t \nabla f(x_n) \cdot p_n \\
&\quad - (A_{\delta t} \gamma - C_{\delta t}) \delta t \|p_n\|^2 + [2B_{\delta t} + C_{\delta t} (\gamma + cR^2)] \delta t \|x_n\| \|p_n\| \\
&\quad + Q \delta t^2 (\|p_n\|^2 + \|\nabla f(x_n)\|^2).
\end{aligned}$$

In order to eliminate the term $\nabla f(x_n) \cdot p_n$, we set $A_{\delta t} = 1$, and we also demand $C_{\delta t} < \gamma$, upon which we have

$$\begin{aligned}
\mathcal{W}(x_{n+1}, p_{n+1}) &\leq \mathcal{W}(x_n, p_n) - C_{\delta t} \delta t x_n \cdot \nabla f(x_n) - (\gamma - C_{\delta t}) \delta t \|p_n\|^2 \\
&\quad + [2B_{\delta t} + C_{\delta t} (\gamma + cR^2)] \delta t \|x_n\| \|p_n\| + Q \delta t^2 (\|p_n\|^2 + \|\nabla f(x_n)\|^2).
\end{aligned}$$

Assuming that $x^* = 0$, $f(x^*) = 0$ (where $\nabla f(x^*) = 0$) and using the strong convexity and Lipschitz continuity assumption we have $f(x) \geq m \frac{\|x\|^2}{2}$ and $\|\nabla f(x)\|^2 \leq M^2 \|x\|^2$. These inequalities imply that there exists $K \in \mathbb{R}_+$ such that

$$\|p\|^2 + \|\nabla f(x)\|^2 \leq K \mathcal{W}(x, p)$$

for $B_{\delta t} > C_{\delta t}^2$. This allows us to upper bound $\mathcal{W}(x_{n+1}, p_{n+1})$ as follows;

$$\begin{aligned}
\mathcal{W}(x_{n+1}, p_{n+1}) &\leq (1 + QK \delta t^2) \mathcal{W}(x_n, p_n) - C_{\delta t} \delta t x_n \cdot \nabla f(x_n) \\
&\quad - (\gamma - C_{\delta t}) \delta t \|p_n\|^2 + [2B_{\delta t} + C_{\delta t} (\gamma + cR^2)] \delta t \|x_n\| \|p_n\|.
\end{aligned}$$

Finally, using the strong convexity assumption and a Cauchy-Schwarz inequality we obtain

$$\begin{aligned}
\mathcal{W}(x_{n+1}, p_{n+1}) &\leq (1 + QK \delta t^2) \mathcal{W}(x_n, p_n) - aC_{\delta t} \delta t f(x_n) \\
&\quad - \left(C_{\delta t} b - \frac{\lambda^2}{2} (2B_{\delta t} + C_{\delta t} (\gamma + cR^2)) \right) \delta t \|x_n\|^2 \\
&\quad - \left((\gamma - C_{\delta t}) - (2B_{\delta t} + C_{\delta t} (\gamma + cR^2)) \frac{1}{2\lambda^2} \right) \delta t \|p_n\|^2.
\end{aligned}$$

Setting $B_{\delta t} = C_{\delta t} = \varepsilon$ and $\lambda^2 = \sqrt{\varepsilon}$, we obtain

$$\begin{aligned}
\mathcal{W}(x_{n+1}, p_{n+1}) &\leq (1 + QK\delta t^2)\mathcal{W}(x_n, p_n) - a\varepsilon\delta t f(x_n) \\
&\quad - \left(\varepsilon b - \frac{\sqrt{\varepsilon}}{2} (2\varepsilon + \varepsilon(\gamma + cR^2)) \right) \delta t \|x_n\|^2 \\
&\quad - \left((\gamma - \varepsilon) - \left(2\varepsilon + \varepsilon(\gamma + cR^2) \right) \frac{1}{2\sqrt{\varepsilon}} \right) \delta t \|p_n\|^2 \\
&= (1 + QK\delta t^2)\mathcal{W}(x_n, p_n) - a\varepsilon\delta t f(x_n) \\
&\quad - \left(\varepsilon b - \varepsilon^{3/2} \left(1 + \frac{1}{2}\gamma + \frac{1}{2}cR^2 \right) \right) \delta t \|x_n\|^2 \\
&\quad - \left(\gamma - \varepsilon - \sqrt{\varepsilon} \left(1 + \frac{\gamma}{2} + \frac{cR^2}{2} \right) \right) \delta t \|p_n\|^2 \\
&\leq (1 - \nu\delta t + QK\delta t^2)\mathcal{W}(x_n, p_n).
\end{aligned}$$

Note we need to choose a sufficiently small $\varepsilon > 0$ such that the coefficient of the $\|x_n\|^2$ and $\|p_n\|^2$ terms remain negative. The above implies that there exists $\nu > 0$ such that

$$\mathcal{W}(x_{n+1}, p_{n+1}) \leq (1 - \nu\delta t + QK\delta t^2)\mathcal{W}(x_n, p_n).$$

Upon choosing sufficiently small step size δt , so that $1 - \nu\delta t + QK\delta t^2 \leq 1$ we obtain $\mathcal{W}(x_{n+1}, p_{n+1}) \leq \mathcal{W}(x_n, p_n) \leq \mathcal{W}_R$. This closes the induction argument. The same result also allows us to conclude exponential convergence of the discrete dynamics. \square

I.4 Convergence of discretized CD dynamics with stochastic gradients

We now show convergence of the discrete CD dynamics in the stochastic gradient setting. We include a stochastic-gradient version only for CD, since the noise shows up only in the gradient term and the proof is very similar to the deterministic case. We do not present a similar proof for iKFAD as the extra variable ξ depends on the (noisy) momentum and feeds back into the momentum update, which in turn adds extra cross-terms to control. We leave the stochastic iKFAD proof for future work.

We use an Euler discretization similarly to (12a), (12b), where the update of the momenta is performed based on the stochastic gradient.

$$\begin{aligned}
p_{n+1} &= (1 - \gamma\delta t)p_n - c\delta t[p_n]^3 - \delta tG(x_n), \\
x_{n+1} &= x_n + \delta t p_n,
\end{aligned}$$

where we assume $\gamma\delta t$ is sufficiently small. We denote by $G(x)$ the stochastic gradient, where $\mathbb{E}[G(x)] = \nabla f(x)$.

Assumption 1. *The variance of the stochastic gradients is uniformly bounded, that is there exists $D > 0$ such that, for all $x \in \mathbb{R}^N$, $\mathbb{E}\|G(x) - \nabla f(x)\|^2 \leq D$.*

Proposition 4. *Assume that $f \in C^2$ and $\exists m, M \in \mathbb{R}_+$ such that $m \leq \nabla^2 f(x) \leq M$ for any $x \in \mathbb{R}^N$. Fix $L > 0$, then, for any initial condition (x_0, p_0) such that*

$$\|x_0\| + \|p_0\| \leq L,$$

there exists $\delta t^ > 0, r > 0$ and $C > 0$ for which*

$$\forall n \geq 0 \text{ and } \forall \delta t \in (0, \delta t^*), \quad \mathbb{E}[f(x_n) - f(x^*)] + \mathbb{E}\|p_n\|^2 \leq C e^{-\kappa n \delta t}.$$

We again consider the Lyapunov function (28)

$$\mathcal{W}(x_n, p_n) = f(x_n) + A_{\delta t} \frac{\|p_n\|^2}{2} + B_{\delta t} \|x_n\|^2 + C_{\delta t} x_n \cdot p_n.$$

We start by upper bounding the expectation of each of the terms in the discrete Lyapunov function. Note that the expectations are conditional on x_n, p_n . We follow the same procedure as in section I.3. As we have assumed that $0 < m < \nabla^2 f(x) \leq M$, we have

$$f(x_{n+1}) \leq f(x_n) + \delta t \nabla f(x_n) \cdot p_n + \frac{\delta t^2 M}{2} \|p_n\|^2,$$

so that

$$\mathbb{E}[f(x_{n+1})] \leq f(x_n) + \delta t \nabla f(x_n) \cdot p_n + \frac{\delta t^2 M}{2} \|p_n\|^2.$$

Next, we can bound the expectation of the squared norm of the momenta (see proof of Theorem 4, Appendix I.3) as:

$$\|p_{n+1}\|^2 \leq \|p_n\|^2 - 2\gamma\delta t \|p_n\|^2 - 2\delta t p_n \cdot G(x_n) + C\delta t^2 (\|p_n\|^2 + \|G(x_n)\|^2),$$

so that, using

$$\begin{aligned} \mathbb{E}[\|G(x_n)\|^2] &= \mathbb{E}\|\nabla f(x_n) + (G(x_n) - \nabla f(x_n))\|^2 \\ &= \|\nabla f(x_n)\|^2 + 2\nabla f(x_n) \cdot \mathbb{E}[G(x_n) - \nabla f(x_n)] + \mathbb{E}\|G(x_n) - \nabla f(x_n)\|^2 \\ &\leq \|\nabla f(x_n)\|^2 + D, \end{aligned}$$

(note that $\mathbb{E}[G(x_n) - \nabla f(x_n)] = \mathbb{E}[G(x_n)] - \nabla f(x_n) = 0$) we obtain

$$\begin{aligned} \mathbb{E}\|p_{n+1}\|^2 &\leq \|p_n\|^2 - 2\gamma\delta t \|p_n\|^2 - 2\delta t p_n \cdot \nabla f(x_n) + C\delta t^2 (\|p_n\|^2 + \mathbb{E}\|G(x_n)\|^2) \\ &\leq \|p_n\|^2 - 2\gamma\delta t \|p_n\|^2 - 2\delta t p_n \cdot \nabla f(x_n) + C\delta t^2 (\|p_n\|^2 + \|\nabla f(x_n)\|^2 + D). \end{aligned}$$

Next, we have:

$$\mathbb{E}\|x_{n+1}\|^2 = \|x_n\|^2 + 2\delta t x_n \cdot p_n + \delta t^2 \|p_n\|^2.$$

Finally

$$\begin{aligned} x_{n+1} \cdot p_{n+1} &\leq x_n \cdot p_n + (\gamma + cR^2)\delta t \|x_n\| \|p_n\| - \delta t x_n \cdot G(x_n) + \delta t \|p_n\|^2 \\ &\quad + C\delta t^2 (\|p_n\|^2 + \|G(x_n)\|^2), \end{aligned}$$

so that

$$\begin{aligned} \mathbb{E}[x_{n+1} \cdot p_{n+1}] &\leq x_n \cdot p_n + (\gamma + cR^2)\delta t \|x_n\| \|p_n\| - \delta t x_n \cdot \nabla f(x_n) + \delta t \|p_n\|^2 \\ &\quad + C\delta t^2 (\|p_n\|^2 + \|\nabla f(x_n)\|^2 + D). \end{aligned}$$

Having derived the above upper bounds, convergence can be shown following the same steps as in Section I.3.